



1 **Mg/Ca and  $\delta^{18}\text{O}$  in multiple species of planktonic foraminifera from 15 Ma to Recent**

2

3

4 Flavia Boscolo-Galazzo<sup>1\*</sup>, David Evans<sup>2</sup>, Elaine M. Mawbey<sup>3</sup>, William R. Gray<sup>4</sup>, Paul N.  
5 Pearson<sup>3,5</sup>, Bridget S. Wade<sup>3</sup>

6 <sup>1</sup>Bremen University, MARUM, Center for Marine Environmental Sciences (Germany);

7 <sup>2</sup>School of Ocean and Earth Science, University of Southampton, European Way, SO14 3ZH,  
8 Southampton (UK);

9 <sup>3</sup>Department of Earth Sciences, University College London, London (UK);

10 <sup>4</sup>Laboratoire des Sciences du Climat et de l'Environnement (LSCE/IPSL), Université Paris-  
11 Saclay, Gif-sur-Yvette (France).

12 <sup>5</sup>School of Earth and Environmental Sciences, Cardiff University, Cardiff (UK)

13 \*Corresponding author: [fboscologalazzo@marum.de](mailto:fboscologalazzo@marum.de)

14 [D.evans@soton.ac.uk](mailto:D.evans@soton.ac.uk)

15 [mawbeye@gmail.com](mailto:mawbeye@gmail.com)

16 [william.gray@lsce.ipsl.fr](mailto:william.gray@lsce.ipsl.fr)

17 [p.pearson@ucl.ac.uk](mailto:p.pearson@ucl.ac.uk)

18 [b.wade@ucl.ac.uk](mailto:b.wade@ucl.ac.uk)

19

20

21 **Abstract**

22 The ratio of the trace element Mg over Ca (Mg/Ca) and the oxygen isotopic composition ( $\delta^{18}\text{O}$ ) of  
23 foraminiferal calcite are widely employed for reconstructing past ocean temperatures, although  
24 geochemical signals are also influenced by several other factors that vary temporally and spatially.  
25 Here, we analyze a global dataset of Mg/Ca and  $\delta^{18}\text{O}$  data of 59 middle Miocene to Holocene  
26 species of planktonic foraminifera from a wide range of depth habitats, many of which have never  
27 been analyzed before for Mg/Ca. We investigate the extent to which Mg/Ca and  $\delta^{18}\text{O}$  covary



28 through time and space, and identify several sources of mismatch between the two proxies. Once  
29 the data are adjusted for long term non-thermal factors, Mg/Ca and  $\delta^{18}\text{O}$  are overall positively  
30 correlated in a way consistent with temperature being the dominant controller of both through  
31 space and time and across many different species, including deep-dwellers. However, we identify  
32 several species with systematic offsets in Mg/Ca values, to which multispecies calibrations should  
33 be applied with caution. We can track the appearance of such offsets through ancestor-descendent  
34 species over the last 15 million years and propose that the emergence of these offsets may be the  
35 geochemical expression of evolutionary innovations. We find virtually all of the Mg/Ca and  $\delta^{18}\text{O}$ -  
36 derived temperatures from the commonly used genera *Globigerinoides* and *Trilobatus* are within  
37 uncertainty of each other, highlighting the utility of these species for paleoceanographic  
38 reconstructions. Our results highlight the potential of leveraging information from species lineages  
39 to improve sea surface temperature reconstruction from planktonic foraminifera over the  
40 Cenozoic.

## 41 **1. Introduction**

42 Geochemical analyses of foraminifera are commonly applied to reconstruct paleoceanographic  
43 conditions, such as marine temperatures, and therefore infer past climatic changes. In particular,  
44 the fossil tests of planktonic foraminifera (calcareous zooplankton) provide one of the most widely  
45 used paleoclimate archives. Here we focus on two of these parameters:  $\delta^{18}\text{O}$  and Mg/Ca, both of  
46 which have been used widely as temperature proxies.

47 The oldest and possibly most widely utilized of these proxies is the ratio of oxygen isotopes in  
48 their calcite test which, due to slight differences in reactivity of molecules containing the different  
49 isotopes, is temperature-dependent (Urey, 1947; see Pearson, 2012 for review). This effect has  
50 been quantified in experiments with inorganic calcite (e.g., Kim and O'Neill, 1997) and planktonic



51 foraminifera in culture (e.g., Erez and Luz, 1983; Bemis et al., 1998). Tests of planktonic  
52 foraminifera calcifying in warmer waters are depleted in  $^{18}\text{O}$  relative to species living in cooler  
53 waters (Emiliani, 1954). A second, more recently established paleoclimate proxy is the ratio of  
54 magnesium to calcium in test calcite (Chave 1954; Nürnberg et al., 1996). During inorganic  
55 precipitation experiments, the Mg/Ca ratios of calcite were found to be higher at greater  
56 temperatures (Mucci, 1987). This relationship led to the in-depth exploration of Mg/Ca ratios in  
57 planktonic and benthic foraminifera and its potential application as a temperature proxy through  
58 culturing (Lea et al., 1999; von Langen et al., 2005), core top (Nürnberg, 1995; Elderfield and  
59 Gassen, 2000) and sediment trap studies (Anand et al., 2003).

60 As they represent two different chemical systems, the Mg/Ca and oxygen stable isotope ratios in  
61 foraminifera are often used together as independent temperature proxies. For instance,  $\delta^{18}\text{O}$   
62 derived calcification temperatures have been combined with Mg/Ca data to derive Mg/Ca  
63 temperature calibrations (e.g., Anand et al., 2003; McConnel and Thunell, 2005; Mohtadi et al.,  
64 2009). Other studies have applied these two systems together to infer the influence of  
65 environmental parameters such as seawater salinity on Mg/Ca (e.g., Mathien-Blard and Bassinot,  
66 2009; Hönisch et al., 2013) and global ice volume (e.g., Lear et al., 2000; Katz et al., 2008). Works  
67 such as these assume covariance of the two proxies for any given sample, which should be the case  
68 if both systems are impacted purely by calcification temperature. Nonetheless, there are known  
69 non-thermal effects influencing both Mg/Ca and  $\delta^{18}\text{O}$ . For oxygen isotope values, these include  
70 the oxygen isotopic composition of seawater ( $\delta^{18}\text{O}_{\text{sw}}$ ) and to a lesser degree, seawater pH or  
71 carbonate ion concentration (Spero et al., 1997; Zeebe, 1999). Seawater carbonate chemistry has  
72 also been shown to impact the Mg/Ca proxy. Culture and sediment trap studies demonstrate surface  
73 ocean seawater pH can influence Mg/Ca in planktonic foraminifera (Lea et al 1999; Evans et al.,



74 2016a; Gray et al 2018), with the sensitivity of Mg/Ca to pH appearing to vary between species  
75 (Gray and Evans 2019). Mg/Ca values of foraminifera are also dependent on the Mg/Ca of  
76 seawater (Evans et al., 2016b), and both oxygen isotope and Mg/Ca values can be impacted by test  
77 recrystallization (Dekens et al., 2002). Mg/Ca values are susceptible to the preferential loss of Mg  
78 during dissolution, and are thus influenced by the calcite saturation state of bottom waters  
79 (Regenberg et al 2014; Tierney et al 2019). Seawater salinity has a minor secondary effect on  
80 Mg/Ca values (Kisakürek et al., 2008, Hönisch et al., 2013) and whilst salinity has little direct  
81 effect on oxygen isotopes, a change in salinity is usually accompanied by a change in  $\delta^{18}\text{O}_{\text{sw}}$   
82 because hydrological processes such as evaporation and precipitation are closely coupled  
83 (LeGrande and Schmidt 2006). Lastly, so-called ‘vital effects’, which lump together a wide variety  
84 of species-specific processes such as metabolism (including the process of calcification and the  
85 incorporation of metabolic products), the position within the water column and life cycle depth  
86 migration, the presence of photosymbionts, and seasonality (see summary in Schiebel and  
87 Hemleben, 2017), also add complexity to the interpretation of both the oxygen isotope and Mg/Ca  
88 proxies.

89 Here we use the dataset published in Boscolo-Galazzo, Crichton et al., (2021), to examine  
90 covariance between Mg/Ca and  $\delta^{18}\text{O}$  in planktonic foraminifera extracted from sediments across  
91 a wide range of geographic locations, time intervals, and species. The dataset is composed of  $\delta^{18}\text{O}$   
92 and Mg/Ca data measured on 59 species of planktonic foraminifera, of which 24 have never before  
93 been measured for Mg/Ca (Supplementary Tables 1, 2). The data are from different ocean basins  
94 and latitudes and a range of ages between the middle Miocene (~15 million years ago, Ma) and  
95 the Holocene. Paired Mg/Ca and  $\delta^{18}\text{O}$  were measured on the same samples, hence this dataset is  
96 ideally suited to isolate potential ecological, environmental and preservational factors which may



97 imprint Mg/Ca or  $\delta^{18}\text{O}$  or both, and which are otherwise impossible to recognize in studies  
98 focusing on a limited number of species, a narrow study area or time interval. In particular, it  
99 provides the unique opportunity to simultaneously: (1) compare coupled  $\delta^{18}\text{O}$  and Mg/Ca data on  
100 a broader than usual geographical and temporal scale; (2) Compare coupled  $\delta^{18}\text{O}$  and Mg/Ca data  
101 across species of different ecologies; (3) Evaluate Mg/Ca data of extinct species against those of  
102 their modern descendants; (4) Test whether temperature can still be recognized as predominantly  
103 driving covariance in the dataset when spatial, temporal and ecological variables are  
104 simultaneously in play.

## 105 **2. Material and Analytical methods**

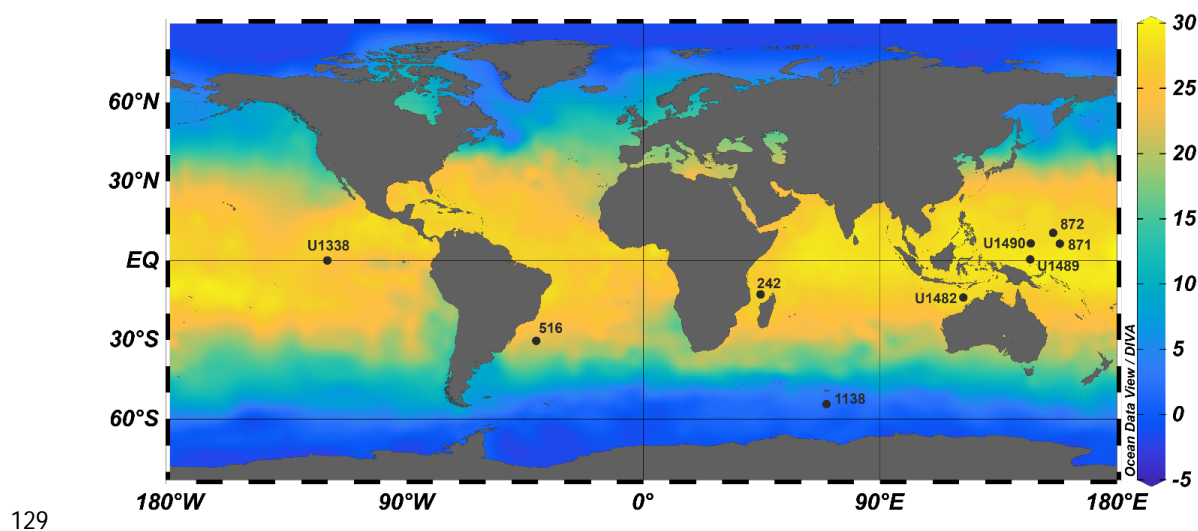
### 106 2.1 Material

107 The dataset (Boscolo-Galazzo, Crichton et al., 2021) was produced from a range of globally and  
108 latitudinally distributed DSDP (Deep Sea Drilling Program), ODP (Ocean Drilling Program), and  
109 IODP (Integrated Ocean Drilling Program/International Ocean Discovery Program) sites (Fig. 1)  
110 which are high in carbonate and composed of calcareous nannofossils and foraminiferal pelagic  
111 oozes, with some input of siliceous plankton. Sites were selected based on the best available global  
112 and temporal coverage and preservation of foraminifera. Planktonic foraminiferal preservation  
113 ranges from excellent to very good (recrystallized but lacking overgrowth and infilling) (Boscolo-  
114 Galazzo, Crichton et al., 2021) with the exception of Sites U1490 and U1489, where there is some  
115 overgrowth and infilling in the middle Miocene (Fayolle and Wade, 2020; Boscolo-Galazzo,  
116 Crichton et al., 2021). The target time intervals selected for sampling were 0, 2.5, 4.5, 7.5, 10, 12.5  
117 and 15 Ma. Biostratigraphic analysis was used to assess age using the biochronology of Wade et  
118 al. (2011) calibrated to the time scale of Lourens et al. (2004) (Supplementary Table 1).



119 2.2 Planktonic foraminifera

120 Fifty-nine species of planktonic foraminifera were analysed for Mg/Ca and  $\delta^{18}\text{O}$ . Planktonic  
121 foraminiferal were picked from three constrained size fractions: 180-250  $\mu\text{m}$ , 250-300  $\mu\text{m}$  and  
122 300-355  $\mu\text{m}$ . Planktonic foraminiferal geochemistry can change through size (e.g., Birch et al.,  
123 2013), so here we used data from the size fraction 250-355  $\mu\text{m}$  only, giving a total of 57 species  
124 in the dataset. For abundant species, up to 80 specimens were picked for geochemical analysis,  
125 with as many as possible picked in the case of less common species. Hence, our foraminiferal data  
126 represent an average from multiple specimens. Paleodepth habitat attributions follow Boscolo-  
127 Galazzo, Crichton et al. (2021) and Boscolo-Galazzo et al. (2022). Planktonic foraminiferal  
128 taxonomy follows the concepts described in Boscolo-Galazzo et al. (2022).



129  
130 **Figure 1.** Site map with present-day mean annual sea surface temperatures ( $^{\circ}\text{C}$ ) from the World  
131 Ocean Atlas 2013 (Locarnini et al., 2013).

132

133



134 2.3 Trace element and stable isotope analysis

135 Picked planktonic foraminifera were crushed between two glass slides to open all large chambers.  
136 When there was enough material, the crushed sample was split for stable isotope and trace element  
137 analysis. The trace element split was cleaned using a protocol to remove clays and organic matter  
138 (step A1.1-A1.3 of Barker et al. (2003)). The samples did not undergo reductive cleaning due to  
139 their fragility and small sample size, and because the reductive step may cause preferential removal  
140 of high Mg/Ca calcite from the test (Yu et al., 2007). Samples were dissolved in trace metal pure  
141 0.065 M HNO<sub>3</sub>, then diluted with trace metal pure 0.5 M HNO<sub>3</sub> and analysed at Cardiff University  
142 on a Thermo Fisher Scientific Element XR ICP-MS against standards with matched calcium  
143 concentration to reduce matrix effects (Lear et al., 2002). Long term analytical precision  
144 determined from consistency standards (CS1 and CS2) with Mg/Ca ratios of 1.24 mmol/mol and  
145 7.15 mmol/mol are ~0.7 and ~0.8% (relative standard deviation). Mg/Ca was plotted against Fe/Ca  
146 and Mn/Ca to assess whether there was any relationship as a result of the presence of Fe-Mn  
147 oxyhydroxides affecting Mg/Ca, but there was no correlation between the contaminant indicators  
148 and Mg/Ca (Supp. Fig. 1).

149 Stable isotopes were measured on a Delta V Advantage with Gasbench II mass spectrometer at the  
150 Cardiff University stable isotope facility. Stable isotope results were calibrated to the VPDB scale  
151 using an in-house carbonate standard (Carrara marble). Analytical precision was 0.05‰ for δ<sup>18</sup>O  
152 and 0.05‰ for δ<sup>13</sup>C.

153 2.4 Data analysis



154 Before performing the analysis, we screened the dataset for outliers, and removed one anomalously  
155 high datapoint with a Mg/Ca value  $>9$  mmol/mol which we attributed to analytical error  
156 (Supplementary Table 1).

#### 157 2.4.1 Formulation of theoretical relationships between Mg/Ca and $\delta^{18}\text{O}$

158 To test for covariation between Mg/Ca and oxygen isotope data, we regressed the data against each  
159 other and compared the observed relationship with that expected from modern calibrations. We  
160 did this to initially explore the dataset and what kind of relationship we might expect between  
161 Mg/Ca and  $\delta^{18}\text{O}$  and whether this manifests in the dataset, before applying corrections for the non-  
162 thermal influences on both proxies. Given the complexity of the sample set (e.g., multiple species,  
163 ages, locations, preservation), different expected relationships between Mg/Ca and  $\delta^{18}\text{O}$  are  
164 possible, which depend on: i) species-specific vital effects, ii) the non-thermal controls on Mg/Ca,  
165 (salinity, pH, Mg/Ca<sub>sw</sub>), iii) non-thermal controls on  $\delta^{18}\text{O}$  (pH/[CO<sub>3</sub><sup>2-</sup>]),  $\delta^{18}\text{O}_{\text{sw}}$ , as well as how  
166 these factors change through time. To account for this, we calculated a number of possible  
167 expected theoretical relationships to give a sense of how much of the scatter in the raw data is  
168 likely to be explicable by these factors and inform our following data-analysis accordingly. We  
169 stress that this exercise was conducted as a mean of exploring the whole data set; no single  
170 relationship will be able to explain the dataset because it is influenced by multiple, often  
171 interlinked, variables.

172 Expected theoretical relationships were calculated starting with modern laboratory culture  
173 calibrations, onto which the key non-thermal long-term and spatial controls on these proxies were  
174 sequentially added to demonstrate how much each of these is expected to shift the slope of the  
175 expected Mg/Ca- $\delta^{18}\text{O}$  relationship (Fig. 2A). Specifically, we i) combined the calibrations for  
176 *Globigerinoides ruber* and *Trilobatus sacculifer* of Gray & Evans (2019) with the  $\delta^{18}\text{O}$ -





177 temperature equation of Erez & Luz (1983), ii) added the impact of a 0.15 unit whole ocean pH  
178 change (approximating the magnitude of the Neogene whole ocean change, e.g., Rae et al., 2021)  
179 using the pH-Mg/Ca slope for *G. ruber* as an example (note that this is only applicable to species  
180 that show a pH sensitivity) (Evans et al., 2016a), iii) included the expected control of temperature  
181 on pH via the T-dependent dissociation of water ( $K_w$ ), i.e., temperature-driven pH changes within  
182 a given time interval independent of whole ocean pH shifts (Gray et al., 2018), iv) showed the  
183 impact of  $Mg/Ca_{sw}$  half of the modern ratio (Evans et al., 2016b), v) included the effect of pH or  
184  $[CO_3^{2-}]$  on  $\delta^{18}O$  (Spero et al., 1997; Zeebe, 1999) given the covariance of temperature and pH  
185 described in point iii above using the multispecies average slope of Gaskell et al. (2023), and  
186 finally vi) explored the likely impact of the covariance of  $\delta^{18}O_{sw}$  and temperature that is  
187 characteristic of the modern ocean and arises from the broad coupling of the hydrological cycle  
188 with surface temperatures. Specifically, this latter influence was calculated by combing SST data  
189 from the 2013 World Ocean Atlas (Locarnini et al., 2013) and  $\delta^{18}O_{sw}$  from LeGrande & Schmidt  
190 (2006), taking all surface ocean data except that from polar meltwater regions, which demonstrates  
191 that, on average, in the modern ocean  $\delta^{18}O_{sw}$  increases by 0.0425 ‰ per °C SST increase.

192 Each of these factors was applied additively such that (e.g.) the fourth factor listed above  
193 ( $Mg/Ca_{sw}$ ) in Fig. 2 includes numbers 1 through 3. The sum of the influence of these factors on  
194 the theoretical  $\delta^{18}O$ -Mg/Ca relationship is represented by the thick blue line in Figure 2A and the  
195 black line in Figures 3, 6, 7 and 8, which has a slope of  $-2.08$  in  $\delta^{18}O$ - $\ln(Mg/Ca)$  space.

196 The magnitude of some of these potential non-thermal controls on the two proxies over the time  
197 interval studied here are reasonably well constrained. Specifically, the long-term whole ocean pH  
198 and  $Mg/Ca_{sw}$  changes are sufficiently well known (Rae et al., 2021; Zhou et al., 2021; Brennan et  
199 al., 2013) that they can be “subtracted” out of the raw proxy values, given that they are likely to



200 apply to all or most species in the dataset. As such, we next explored the degree to which the  
201 Mg/Ca- $\delta^{18}\text{O}$  covariation improves once long-term whole ocean pH and Mg/Ca<sub>sw</sub> changes are  
202 removed. To avoid (possibly incorrect) a-priori assumptions regarding, for example, which  
203 Mg/Ca-temperature calibration should be applied to each species in the dataset and the degree to  
204 which surface ocean  $\delta^{18}\text{O}_{\text{sw}}$  has varied at the study sites, we initially did this keeping the Mg/Ca  
205 and  $\delta^{18}\text{O}$  comparison in raw proxy space and: 1) converted the raw Mg/Ca values to temperature  
206 using the multispecies Mg/Ca-temperature calibration from Gray and Evans (2019), together with  
207 our best estimate of pH and Mg/Ca<sub>sw</sub> (as described below (§2.4.2)), and 2) converted the  
208 temperatures back into Mg/Ca using the same calibration but modern seawater Mg/Ca and pH. In  
209 addition, we subtracted out the long-term whole ocean change in  $\delta^{18}\text{O}_{\text{sw}}$  related to continental ice  
210 growth using the sea level curve of Rohling et al. (2021) and a sea level- $\delta^{18}\text{O}_{\text{sw}}$  scaling factor of  
211 1‰ per 67 m. This results in a raw proxy dataset in which the aforementioned long-term non-  
212 thermal factors are no longer present and which can be used to evaluate the occurrence of residual  
213 scatter independent of the long term non-thermal controls on Mg/Ca and  $\delta^{18}\text{O}$  (Fig. 2B).

#### 214 2.4.2 Transformation of proxy values into paleotemperature

215 Measured foraminifera Mg/Ca was transformed into paleotemperature using the *MgCaRB* tool  
216 (Gray & Evans, 2019; <https://github.com/willyrgray/MgCaRB> (R);  
217 <https://github.com/dbjevens/MgCaRB> (Matlab)) which takes into account:

- 218 - Salinity. Although this has a minor effect on Mg/Ca (Hönisch et al., 2013), whole ocean  
219 changes are nonetheless accounted for using a salinity reconstruction derived from scaling  
220 the  $\delta^{18}\text{O}$  benthic stack (Westerhold et al., 2020) to the sea level record of Spratt & Lisiecki  
221 (2016) back to 8 Ma, before which that of Miller et al. (2005) was used, rescaled to match  
222 the  $\delta^{18}\text{O}$ -derived reconstruction at 8 Ma and a sea level of +67 m in an ice-free world at 50



223 Ma. We applied the multispecies salinity sensitivity of Gray & Evans (2019) to all species  
224 (3.6% per salinity unit).

225 - pH. Long-term whole ocean changes were derived from a smoothing spline fit to the boron  
226 isotope-derived pH data compiled by Rae et al. (2021). We applied species-specific pH-  
227 Mg/Ca sensitivities of Gray & Evans (2019) where available for a given species/lineage  
228 (discussed in more detail below) and used the multispecies sensitivity in all other cases.

229 -  $Mg/Ca_{sw}$  was derived by combining the  $[Ca^{2+}_{sw}]$  record of Zhou et al. (2021) with a  
230 smoothing spline fit to the fluid inclusion  $[Mg^{2+}_{sw}]$  data given in Brennan et al. (2013).

231 Raw Mg/Ca values were adjusted using the equation  $Mg/Ca_{corrected} = Mg/Ca_{raw} \times$   
232  $Mg/Ca_{sw}^H/5.2^H$ , where  $H = 0.64$  based on a data compilation of three foraminifera species  
233 and inorganic calcite (Holland et al., 2020; Evans et al., 2015; 2016b; Mucci & Morse,  
234 1983).

235 Because the dataset includes a mix of extant and extinct species, some of these never measured for  
236 trace elements before (Supplementary Table 2), or lacking an extant/well-calibrated modern  
237 relative, when converting Mg/Ca to temperature we started by applying a multispecies equation,  
238 as is typically done for extinct species. Specifically, we used the multispecies Mg/Ca-temperature  
239 equation of Gray & Evans (2019) and applied the multispecies pH, salinity, and temperature  
240 sensitivities, together with the *Globigerinoides ruber* exponential coefficient as most of the species  
241 for which high quality data exist are known to be characterized by a Mg/Ca-pH sensitivity (Lea et  
242 al., 1999; Kisakürek et al., 2008; Evans et al., 2016a). We subsequently applied species-specific  
243 calibrations to selected lineages to explore the degree to which scatter in the dataset can be  
244 accounted for by taking into account phylogenetic relationships among ancestor-descendent  
245 species. Specifically, the *Trilobatus sacculifer* calibration was applied to the *Trilobatus trilobus* -



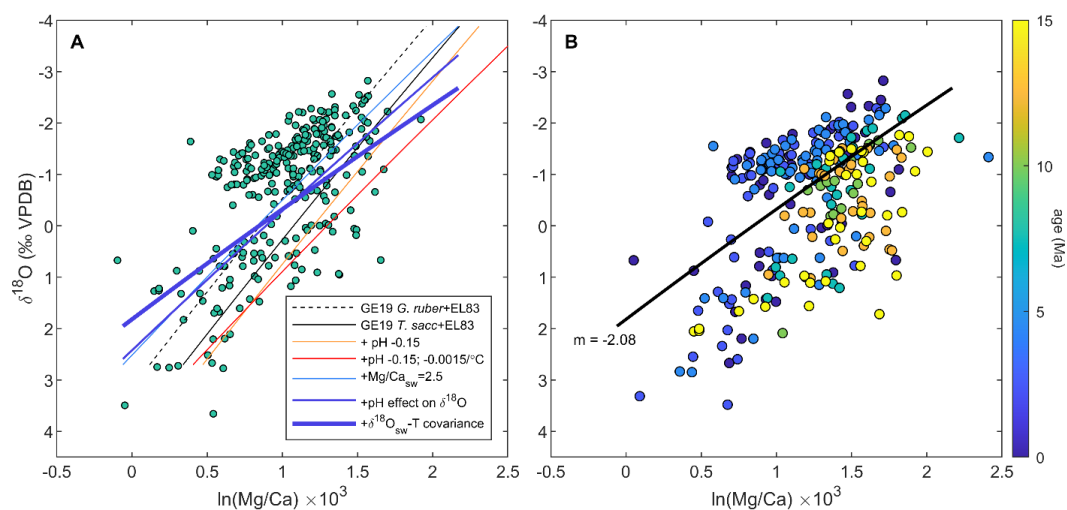
246 *Trilobatus sacculifer* lineage, and the *Orbulina universa* calibration was applied to the  
247 *Preaorbulina-Orbulina* lineage, both from laboratory culture studies following Gray & Evans  
248 (2019). To *Neogloboquadrina* and its descendent lineage *Pulleniatina* we applied a  
249 *Neogloboquadrina pachyderma* calibration with the sensitivities of Tierney et al. (2019)  
250 (implemented with a re-fit to the dataset following the *MgCaRB* approach). We then evaluate the  
251 improvement relative to the multispecies calibration in samples spanning the middle Miocene to  
252 modern. The attribution of phylogenetic relationships follows Aze et al. (2011), Spezzaferri et al.  
253 (2018), Leckie et al. (2018) and Fabbrini et al. (2021). All uncertainties were fully propagated via  
254 Monte Carlo simulation, including those related to: analysis, calibration coefficients, and the 95%  
255 confidence intervals on the salinity, pH, and Mg/Ca<sub>sw</sub> reconstructions, with 10<sup>4</sup> random draws of  
256 each within the uncertainty bounds used to generate the reported values and 95% CI (2.5<sup>th</sup>, 50<sup>th</sup>,  
257 and 97.5<sup>th</sup> percentiles of the resulting dataset).

258 The conversion of  $\delta^{18}\text{O}$  to paleotemperature followed Gaskell et al. (2023) using: the bayfox  
259 calibration (Malevich et al., 2019) and the global and local  $\delta^{18}\text{O}_{\text{sw}}$  of Rohling et al. (2021) and  
260 Gaskell et al. (2023) respectively. The calculation was performed twice, both with and without a  
261 pH/[CO<sub>3</sub><sup>2-</sup>] effect on  $\delta^{18}\text{O}$  (the former using the mean planktonic foraminiferal slope of Gaskell et  
262 al. (2023) and the [CO<sub>3</sub><sup>2-</sup>] record of Zeebe & Tyrrell (2019)).

263 When evaluating the paleotemperature reconstructions, we define whether or not the two proxy  
264 systems agree within uncertainty by determining if the root sum of squares of the two uncertainties  
265 is smaller than the temperature difference between the two proxies. We then proceed to identify  
266 possible drivers for the data deviating from the expected Mg/Ca and  $\delta^{18}\text{O}$  relationship by  
267 evaluating the age of the sample, regional changes in  $\delta^{18}\text{O}$  seawater, depth ecology, and possible  
268 species-specific offsets.



269 We note that all of the above corrections assume surface ocean conditions, while the dataset  
 270 contains a number of species that calcify at depth (Boscolo-Galazzo et al., 2021). Given the  
 271 uncertainties surrounding past changes in vertical pH and  $\delta^{18}\text{O}_{\text{sw}}$  profiles, we do not attempt to  
 272 account for this in our data analysis but note that this consideration should be borne in mind when  
 273 interpreting data from deep-dwelling species.



274

275 **Fig. 2.** Raw  $\delta^{18}\text{O}$  plotted against Mg/Ca for all samples presented here. (A) Several possible expected  
 276 Mg/Ca- $\delta^{18}\text{O}$  slopes are shown for comparison, including that for *G. ruber* and *T. sacculifer* (at constant pH)  
 277 in the modern ocean (solid and dashed black lines respectively). The additive impact of other nonthermal  
 278 controls are then explored using the *G. ruber* calibration as an example, specifically, the impact of: a whole-  
 279 ocean pH shift of 0.15 units (orange line), accounting for the covariation of pH and temperature (driven by  
 280 the temperature-dependent dissociation of water, red line), seawater Mg/Ca half of the present day value  
 281 (thin blue line), the theoretical impact of pH on  $\delta^{18}\text{O}$  (blue line), and the covariance of temperature and  
 282  $\delta^{18}\text{O}_{\text{sw}}$  in the modern ocean (thick blue line). The length of each line depicts the expected Mg/Ca and  $\delta^{18}\text{O}$   
 283 change across the same temperature range in each case (5-35 $^{\circ}\text{C}$ ). All calculations assume  $\delta^{18}\text{O}_{\text{sw}} = 0\text{‰}$ . (B)  
 284 As in panel A, except with the long-term whole ocean changes in pH, Mg/Ca<sub>sw</sub>, and  $\delta^{18}\text{O}_{\text{sw}}$  subtracted out  
 285 of the raw proxy values (see text, using the multispecies calibration of Gray & Evans (2019) in the case of  
 286 the Mg/Ca corrections), i.e., accounting for the impact of these non-thermal Mg/Ca and  $\delta^{18}\text{O}$  controls.  
 287 Sample age is shown as a function of colour.

288

289

290

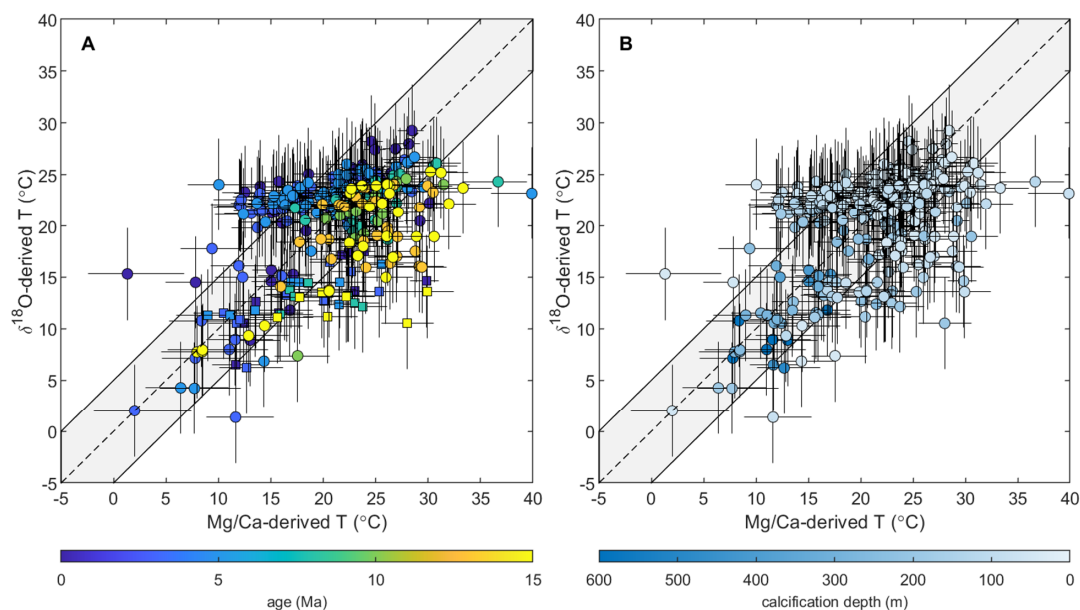


291 **3. Results**

292 Our basic expectation is that higher Mg/Ca should relate to more negative  $\delta^{18}\text{O}$  values for warmer  
293 temperatures, and *vice versa* for colder temperatures. Despite the large number of variables  
294 included, the dataset as a whole shows a significant correlation (Fig. 2A;  $R^2 = 0.37$ , RMSE = 1.01,  
295  $p \ll 0.01$ ) between  $\delta^{18}\text{O}$  and  $\ln(\text{Mg}/\text{Ca})$ . Hence, the  $\delta^{18}\text{O}$ -Mg/Ca covariance can be considered a  
296 robust feature over the past 15 Myr for the majority of the species analyzed and across the study  
297 sites. Nonetheless, there is a high degree of scatter in the data which suggests that the temperature  
298 signal which should lead Mg/Ca and  $\delta^{18}\text{O}$  data to change consistently in opposite directions is  
299 affected by other factors. Our exercise of generating theoretical Mg/Ca- $\delta^{18}\text{O}$  relationships (Fig.  
300 2A), exploring how the relationship between the two proxies might change through space and time,  
301 provides a qualitative indication as to whether the scatter can be attributed to long term non-  
302 thermal factors generally corrected for when using the  $\delta^{18}\text{O}$  and Mg/Ca proxies. The substantial  
303 differences between these expected relationships suggests that this is likely to be the case (Fig.  
304 2A). In particular, Fig. 2A suggests that both a pH effect and  $\text{Mg}/\text{Ca}_{\text{sw}}$  changes through time may  
305 explain a substantial degree of the variability observed in the dataset compared to the modern  
306 relationships (compare the coloured and black lines). Nonetheless, accounting for these long-term  
307 biases alone in the raw dataset does not remove the scatter (Fig. 2B), suggesting the importance of  
308 additional factors, such as vital effects and regional variations in  $\delta^{18}\text{O}_{\text{sw}}$ . Therefore, we next  
309 convert the raw proxy values into temperature including a correction for regional variations in  
310  $\delta^{18}\text{O}_{\text{sw}}$ . Data converted into temperature, along with 95% confidence intervals, are shown in  
311 Figure 3. In this plot 62% of the data points fall within uncertainty, confirming that a high degree  
312 of variability in the raw data can be effectively explained and accounted for by correcting for the  
313 known spatially and temporally varying non-thermal effects influencing both proxies.



314



315

316 **Fig. 3.**  $\delta^{18}\text{O}$  versus Mg/Ca-derived paleotemperatures plotted as function of age (A) and calcification depth  
 317 (B), accounting for the impact of whole ocean and regional changes in  $\delta^{18}\text{O}_{\text{sw}}$  following Gaskell *et al.* [2022]  
 318 and the bayfox  $\delta^{18}\text{O}$ -temperature calibration [Malevich *et al.*, 2019], whole ocean changes in Mg/Ca<sub>sw</sub> and  
 319 pH on Mg/Ca using *MgCaRB* [Gray & Evans, 2019], and including a pH correction on  $\delta^{18}\text{O}$  using the mean  
 320 planktonic foraminifera slope [Gaskell *et al.*, 2023]. Fully propagated uncertainties in both proxies are  
 321 shown, incorporating analysis, calibration, pH, Mg/Ca<sub>sw</sub>,  $\delta^{18}\text{O}_{\text{sw}}$ /salinity (see text for details). Site 516 data  
 322 are shown with square symbols in panel A.

323

324 We find that deep-dwelling and surface-dwelling species fall within uncertainty in terms of the  
 325 broad degree of agreement between Mg/Ca and  $\delta^{18}\text{O}$  derived temperatures, hence different depth-  
 326 habitat ecologies or calcification environments do not represent a systematic source of offset *per*  
 327 *se* (Fig. 3B). Indeed, all the species displaying a temperature offset between the two proxies are  
 328 surface-dwellers (0-200 m depth, Boscolo-Galazzo *et al.*, 2022), with deep-dwellers characterized  
 329 by inter-proxy agreement in almost all cases (Fig. 3B). Additional explanations are required for  
 330 those temperature reconstructions that, all non-thermal and spatial controls included, still plot  
 331 outside their propagated error uncertainty. The data points outside the combined proxy



332 uncertainties either display  $>5^{\circ}\text{C}$  warmer (colder)  $\delta^{18}\text{O}$  (Mg/Ca) temperatures (upper left area of  
333 the plot) or  $>5^{\circ}\text{C}$  warmer (colder) Mg/Ca ( $\delta^{18}\text{O}$ ) temperatures (bottom right area of the plot) (Fig.  
334 3). Figure 3A clearly shows that the large majority of the outliers in the upper left part of the plot  
335 (warmer  $\delta^{18}\text{O}$  temperatures or cooler Mg/Ca temperatures) are species of late Miocene to modern  
336 age, while the outliers in the bottom right part of the plot (warmer Mg/Ca temperatures) are mostly  
337 older species of middle Miocene age or from mid-latitude Site 516 (squares in Fig. 3C). We suggest  
338 and discuss possible main sources for these offsets between Mg/Ca and  $\delta^{18}\text{O}$  temperatures below.

#### 339 **4. Discussion**

##### 340 4.1 Diagenesis

341 Diagenesis is known to alter the test chemistry of foraminifera in three main ways: partial  
342 dissolution, overgrowth, and recrystallization (Edgar et al., 2015). The trace element and isotopic  
343 composition of tests react differently to these diagenetic processes. The trace element composition  
344 of foraminiferal calcite may be susceptible to partial dissolution because it is inhomogeneous  
345 (Fehrenbacher et al., 2014), which decreases trace element ratios in species with high and low-Mg  
346 regions (Dekens et al., 2002; Edgar et al., 2015; Rongstad et al., 2017), resulting in lower  
347 temperature reconstructions. Overgrowth and recrystallization have been shown to add both low-  
348 Mg and high-Mg diagenetic calcite, potentially impacting the original signal in opposite directions  
349 (Branson et al., 2015), although Mg/Ca is relatively robust to this type of diagenesis, at least in  
350 certain circumstances (Staudigel et al., 2022). The oxygen isotopic composition of planktonic  
351 foraminiferal tests is well known to be very sensitive to overgrowth and recrystallization (e.g.  
352 Sexton et al., 2006), whereby the addition of diagenetic calcite, or the replacement of the original  
353 calcite with diagenetic calcite precipitated at the seafloor, can significantly alter the original  
354 isotopic signal shifting it to more positive values (Pearson, 2012; Edgar et al., 2015).





355 The Boscolo-Galazzo, Crichton et al. (2021) dataset spans 15 million years and includes sites with  
356 different average preservation of foraminiferal tests and oceanographic settings. When the data are  
357 regressed against each other (Fig. 2B), we find a total of 26 data points characterized by oxygen  
358 isotope values more positive than expected from their Mg/Ca values (Fig. 2B; Supplementary  
359 Table 1), resulting in  $\delta^{18}\text{O}$  temperatures  $>5^\circ\text{C}$  colder than Mg/Ca temperatures (outside the error  
360 envelope) (Fig. 3; Supplementary Table 1). Twenty-one of these data points were from the older  
361 time slices (12.5 and 15 Ma), one from the 7.5 Ma time slice and four from the core-top of Site  
362 U1338 (Supplementary Table 1).

363 As the majority of these datapoints were characterized by Mg/Ca values of  $\sim 1.5\text{-}2 \ln(\text{Mg}/\text{Ca})$  (Fig.  
364 2B), this yielding more reasonable Mg/Ca than  $\delta^{18}\text{O}$  temperatures for these sites/time intervals  
365 (Supplementary Table 1), the observed offset is most likely best attributed to diagenetic  
366 overgrowth/recrystallization, shifting oxygen isotopes towards more positive values without  
367 affecting Mg/Ca to the same extent. A recent study compared typical Mg/Ca- $\delta^{18}\text{O}$  from  
368 recrystallized planktonic foraminifera with chemical diffusive models simulating early diagenetic  
369 processes in calcite (Staudigel et al., 2022). According to that study, in a closed system, the bulk  
370  $\delta^{18}\text{O}$  value will be altered faster than the Mg/Ca, regardless of what partitioning coefficient is used  
371 for Mg, leading to a progressive shift to more positive  $\delta^{18}\text{O}$  values leaving Mg/Ca virtually  
372 unchanged (Staudigel et al., 2022).

373 The datapoints presenting  $\delta^{18}\text{O}$  overprinted by overgrowth/recrystallization were distributed  
374 across most of the study sites (except for Sites 871/872), but they were more common at Site  
375 U1490 and U1489 (15/26) which are characterized by inferior preservation compared to the others  
376 (Boscolo-Galazzo, Crichton et al., 2021). The core-top samples at Site U1338 show clear signs of  
377 dissolution with highly fragmented tests. These datapoints presented the lowest Mg/Ca values in



378 the dataset (1.68 and 0.91 mmol/mol) with temperatures from Mg/Ca lower than from  $\delta^{18}\text{O}$ . This  
379 suggests that partial dissolution and recrystallization affected both Mg/Ca and  $\delta^{18}\text{O}$  in this sample,  
380 but Mg/Ca more so.

381 Overall, our scrutiny for diagenesis of the Boscolo-Galazzo, Crichton et al., (2021) dataset is  
382 consistent with previous studies suggesting that  $\delta^{18}\text{O}$  values are more easily affected by  
383 recrystallization than Mg/Ca (Sexton et al., 2006; Staudigel et al., 2022; John et al., 2023), similar  
384 to other trace element systems (Edgar et al., 2015).

385 Based on the considerations above we excluded the affected 26 datapoints from the subsequent  
386 analysis as being characterized by a stronger diagenetic overprint than the rest of the dataset  
387 (Supplementary Table 1). Removing the affected datapoints in some but not all the cases equated  
388 to removing a whole sample (Supplementary Table 1). This is because of variable diagenetically  
389 offset  $\delta^{18}\text{O}$  values from different species in a sample, as observed elsewhere (Sexton et al., 2006;  
390 Edgar et al., 2015). The approach used here to reconstruct  $\delta^{18}\text{O}$  temperature shows that for the  
391 majority of the study dataset a diagenetic offset would be comprised within the propagated error  
392 envelope ( $\sim 2\text{--}2.5^\circ\text{C}$ ) (Fig. 3) and comparable or not distinguishable from an offset deriving from  
393 poorly constrained  $\delta^{18}\text{O}_{\text{sw}}$ .

#### 394 4.2 Regional scale spatial heterogeneity in seawater chemistry

395 Once converted into temperatures the dataset shows an overall good agreement of Mg/Ca- $\delta^{18}\text{O}$   
396 data, consistent with temperature being a dominant controller of both proxies through time and  
397 across the broad geographical area investigated (Fig. 3). This suggests that, by and large, the  
398 seawater corrections applied for the local and global changes in ocean chemistry are adequate,  
399 although for one site this may not hold true. Site 516 is a mid-latitude site (south-west Atlantic,



400 30°S) characterized by a modern sea surface temperature around 20°C (Fig. 1), most of the data  
401 points from this site have very positive  $\delta^{18}\text{O}$  values associated with high Mg/Ca (Fig. 2B;  
402 Supplementary Table 1). Once converted, this results in  $\delta^{18}\text{O}$  temperatures that are too cold (12-  
403 17°C) compared to both modern (given long-term warming since the Miocene is not expected at  
404 any of these sites) and the equivalent Mg/Ca temperatures from the same samples, which are  
405 around 21-25°C (Fig. 3A; Supplementary Table 1). We do not attribute this mismatch to diagenesis  
406 for a number of reasons. First, Site 516 is characterized by a very good test preservation, much  
407 better than at Site U1489 and U1490 for which diagenesis extensively affects the middle Miocene  
408 samples; second, this mismatch is observed in the entire dataset through samples spanning the  
409 middle Miocene to modern; third, the mismatch is observed for surface-dwelling species only,  
410 with deep-dwellers characterised by  $\delta^{18}\text{O}$  - Mg/Ca in good agreement. Because of its location, Site  
411 516 is situated in an area of complex surface hydrography, as it sits at the confluence between the  
412 warm Brazil Western Boundary Current and the cold Falkland (Malvinas) Current spinning off  
413 from the Antarctic Circumpolar Current (e.g., Jonkers et al., 2021). Compared to the subtropical  
414 gyres, where many of the study samples come from, a large degree of spatial variability of surface  
415 water physical-chemical properties can be expected on a seasonal and multiannual scale. As such,  
416 we suggest that the mismatch between  $\delta^{18}\text{O}$  and Mg/Ca observed in surface dwelling species at  
417 Site 516 may result from changeable surface water properties from the mixing of two very different  
418 water masses creating deviations in pH, salinity and  $\delta^{18}\text{O}_{\text{sw}}$  beyond those that are typical in  
419 stratified open ocean environments and that are difficult to correct for. Sites with a changeable  
420 hydrography such Site 516, may hence not be ideal for the application of geochemical proxies  
421 affected by seawater chemistry, unless changes in seawater chemistry at the site can be  
422 reconstructed directly.

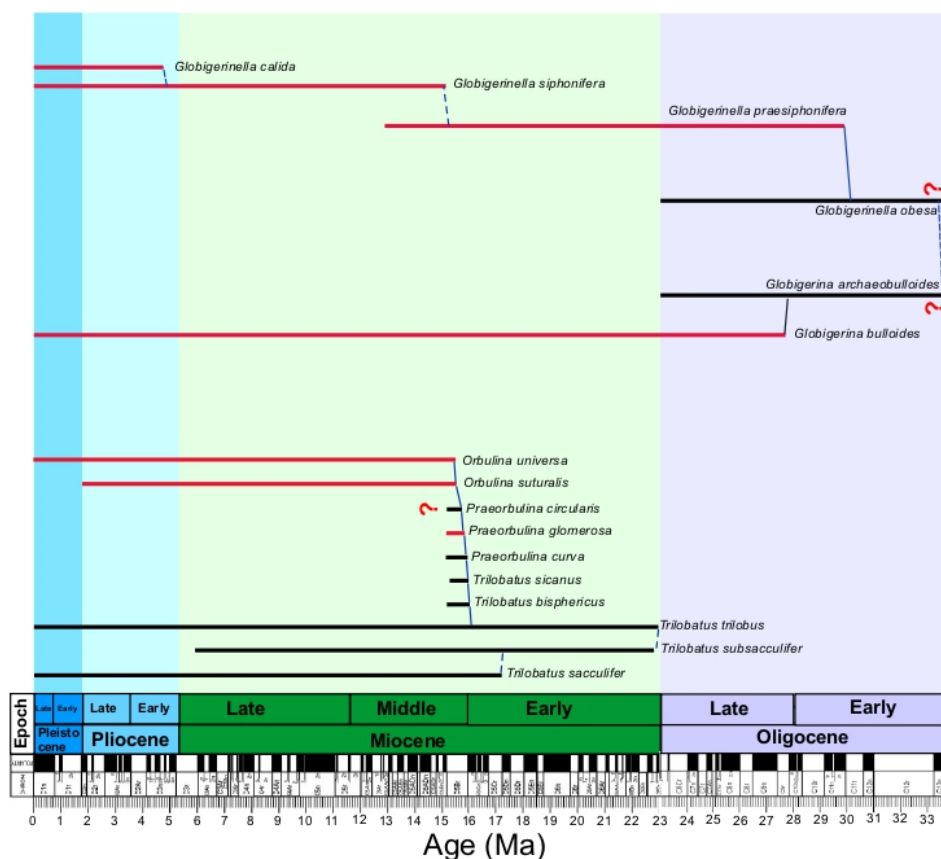


423 4.3 Species-specific offsets

424 The third and largest source of mismatch that we consider is the occurrence of species-specific  
425 offsets, particularly in Mg/Ca given that, in general, the relative degree of inter-species Mg/Ca  
426 variability is greater than for shell oxygen isotope composition (e.g., compare Pearson, 2012; Gray  
427 & Evans, 2019, Regenberg et al., 2009). Here, by the phrase “species-specific offset” we refer to  
428 atypical geochemical signatures which characterize certain species likely as a result of processes  
429 linked to the organism’s metabolism or calcification (i.e., vital effects). When regressing the data  
430 against each other, we find several species presenting systematically offset Mg/Ca values (e.g.,  
431 Fig. 2B; Supplementary Table 1). The occurrence of such offset Mg/Ca values is not evenly  
432 distributed across species, but is shared among related species in both spinose and non-spinose  
433 groups (Figs. 4-5; Supplementary Table 1). Specifically, the spinose offset species *Orbulina*  
434 *universa* (2/5 specimens), *O. suturalis* (3/6) and *Praeorbulina glomerosa* (1/1) present high Mg/Ca  
435 ratios compared to their  $\delta^{18}\text{O}$  values and Mg/Ca of other species (Fig. 6E). We also find that  
436 *Globigerinella siphonifera* (6/7), *G. calida* (1/1), *G. praesiphonifera* (3/4) and *Globigerina*  
437 *bulloides* (5/6) have offset Mg/Ca- $\delta^{18}\text{O}$  values, largely being characterized by higher than expected  
438 Mg/Ca, although three *G. siphonifera* data points show lower Mg/Ca (Figs. 4, 6K; Supplementary  
439 Table 1). Among non-spinose species, offset species are: *Neogloboquadrina humerosa* (11/12), *N.*  
440 *acostaensis* (3/3), *Pulleniatina obliquiloculata* (5/6), *P. praecursor* (3/5), *P. primalis* (4/6),  
441 *Sphaeroidinella dehiscens* (4/4), and *Sphaerodinellopsis paenedehiscens* (5/10), which have  
442 Mg/Ca values lower than expected for their oxygen isotope composition (Figs. 5, 6 G, I;  
443 Supplementary Table 1).

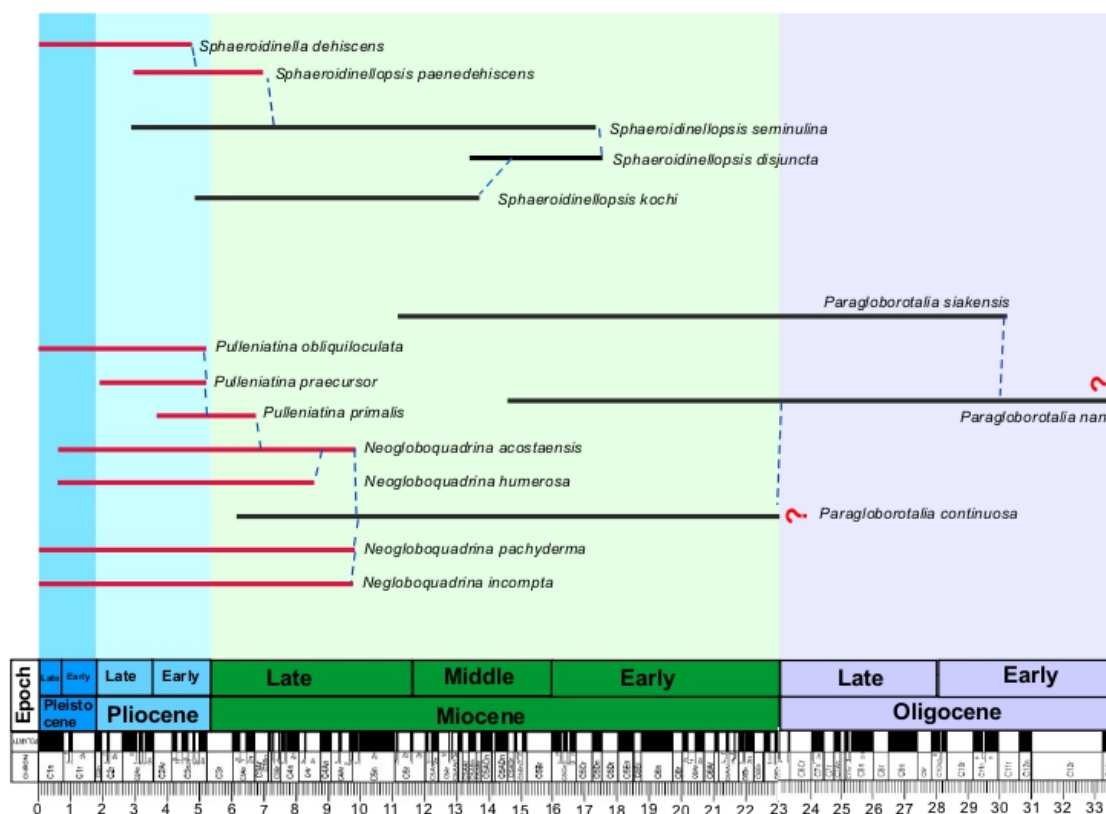


444 These results highlight for the first time the occurrence of similarly offset Mg/Ca values for  
 445 ancestor-descent species belonging to the same lineage as well as, in the case of *Pulleniatina*, to a  
 446 whole lineage descending from *Neogloboquadrina* (Figs. 4-6).



447

448 **Fig. 4.** Phylogenetic relationships of offset spinose-species. Shown here are the species discussed  
 449 in the text, their most closely related species and the ancestors. Red lines indicate species offset in  
 450 Mg/Ca in the study dataset relative to a multispecies calibration approach, black lines indicate non-  
 451 offset species. Red question marks indicate the lack of Mg/Ca data for a given species in the dataset  
 452 presented here. Phylogeny after Aze et al. (2011) and Spezzaferrri et al. (2018). The phylogenetic  
 453 chart was generated using Mikrotax (Huber et al., 2016; www.mikrotax.org/pforams). The  
 454 reference time scale in the figure is the Astronomical time scale of Lourens et al. (2004), until base  
 455 of Chron C6Cn.2n, and Pälike et al. (2006), from top Chron C6Cn.3n until base C13n.



456

457 **Fig. 5.** Phylogenetic relationships of offset non-spinose species. Shown here are the species  
 458 discussed in the text, their most closely related species and the ancestors. Red lines indicate species  
 459 offset in Mg/Ca in the study dataset relative to a multispecies calibration approach, black lines  
 460 indicate non-offset species. Red question marks indicate the lack of Mg/Ca data for a given species  
 461 in the study dataset. Phylogeny after Aze et al. (2011), Leckie et al. (2018) and Fabbrini et al.  
 462 (2021). Phylogeny chart generated using Mikrotax (Huber et al., 2016;  
 463 www.mikrotax.org/pforams). The reference time scale in the figure is the Astronomical time scale  
 464 of Lourens et al. (2004) until base of Chron C6Cn.2n and Pälike et al. (2006), from top Chron  
 465 C6Cn.3n until base C13n.

466

467 Divergent Mg/Ca values for *G. siphonifera* and *O. universa* have previously been reported  
 468 (Opdyke and Pearson, 1995; Anand et al., 2003; Friedrich et al., 2012). In the case of *O. universa*,  
 469 the offset may be related to pH change in the foraminiferal microenvironment due to symbiont  
 470 photosynthetic activity (Eggins et al., 2004) or changes in seawater pH, with Mg/Ca of the test



471 increasing by as much as  $6\pm 3\%$  for each 0.1 unit decrease in pH (Lea et al., 1999; Russell et al.,  
472 2004). pH-related vital effects are reported for other spinose species of planktonic foraminifera  
473 such as *Globigerina bulloides* (Lea et al., 1999; Davis et al., 2017), which is related to the genus  
474 *Globigerinella* (Fig. 4).

475 Among the neogloboquadrinids, *N. acostaensis* and its descendent *N. humerosa* have the most  
476 clearly expressed offset with low Mg/Ca values. In contrast, *Neogloboquadrina pachyderma* and  
477 *N. incompta* are not offset in the study dataset, perhaps simply because of the limited amount of  
478 data (one data point each). More broadly, a Mg/Ca offset compared to other species has been  
479 reported in the literature (Davis et al., 2017). *Neogloboquadrina dutertrei*, *N. incompta*, *N.*  
480 *pachyderma* and *Pulleniatina obliquiloculata* have been shown to be characterized by much lower  
481 trace element concentrations (Mg-Ba-Zn/Ca) in the adult portions of their shells (crust and cortex),  
482 so that a greater amount of adult versus early ontogenetic calcite leads to low trace element values  
483 in bulk shell analysis (Jonkers et al., 2012; Davis et al., 2017; Fritz-Endres & Fehrenbacher, 2021).  
484 The low Mg/Ca of crust and cortex have been found to be independent of ambient temperature in  
485 cultured *Neogloboquadrina* (Davis et al., 2017) and are found in specimens collected both in  
486 surface waters and at depth (Jonkers et al., 2021), indicating that the low Mg/Ca is not acquired  
487 due to calcification in deeper, colder waters of the crust/cortex portion of the shell, although a  
488 greater incidence of crusts is reported for colder waters (Jonkers et al., 2021). In our dataset,  
489 *Neogloboquadrina*, *Pulleniatina* and *Sphaeroidinella/Sphaerodinellopsis* are all characterized by  
490 a thick crust or cortex suggesting their Mg/Ca are biased by low Mg adult calcite being  
491 quantitatively predominant, which is further corroborated by their Mg/Ca being unrelated to  
492 temperature in our data and consistently falling outside of the  $\delta^{18}\text{O}$ -derived temperatures even  
493 accounting for the combined uncertainty of the two proxies (Fig. 6 G-H, I-J).



494 The majority of the data points from the offset spinose and non-spinose species results in  
495 temperature differences between the two proxies greater than 5°C when using the multi-species  
496 calibration from Gray and Evans (2019) as described in §2.4.2, hence outside the calculated error  
497 envelope taking all the non-thermal factors discussed above into account (Fig. 6). A similar  
498 temperature offset is not apparent for other lineages such *Trilobatus trilobus* – *Trilobatus*  
499 *sacculifer* and *Globigerinoides subquadratus* – *G. ruber*, to which the same treatment to the offset  
500 spinose and non-spinose species was applied (§2.4.2, Figs. 6 A-D). Hence, we attribute the offset  
501 temperatures to the atypical Mg/Ca signatures described above in the affected species, in turn  
502 resulting from biology/ecology dependent vital effects shared within a lineage and between related  
503 lineages (Figs. 4-5).

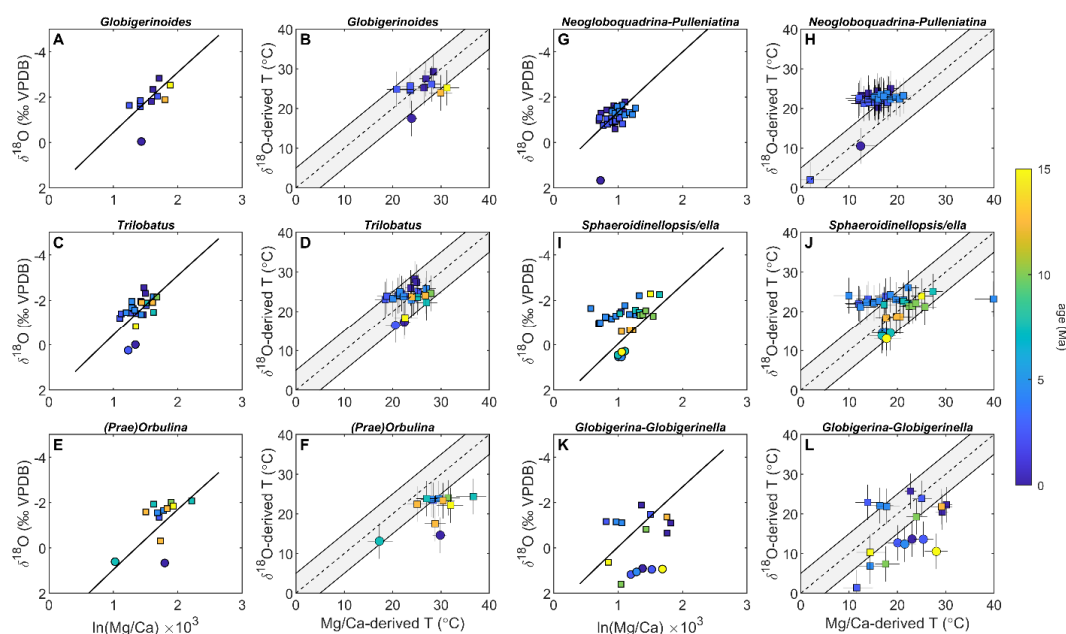
504 When a species-specific calibration for *Neogloboquadrina pachyderma* is applied to descendent  
505 species/lineages and sister taxa (Fig. 5) the offset is successfully corrected for all the  
506 *Neogloboquadrina* and *Pulleniatina* species which effectively no longer produce offset  
507 temperatures (Figs. 6, 7). *Vice versa*, we only observe a minor improvement when applying the  
508 *Orbulina universa* calibration to the *Praeorbulina-Orbulina* lineage, with most temperature data  
509 points remaining offset (Figs. 6, 7), albeit in the opposite direction. This may imply that the *O.*  
510 *universa* laboratory calibrations require revision for application to fossil samples. No large  
511 difference is observed when applying the *Trilobatus sacculifer* calibration to ancestor-descendent  
512 species in the genus *Trilobatus* (Figs. 5-7) although we recommend doing so, given that no Mg/Ca-  
513 pH effect is known for this genus, in contrast to (e.g.) *G. ruber*.

514 Overall, this exercise demonstrates that the majority of the data points characterized by proxy-  
515 proxy disagreement (Fig. 3) are from the lineages: *Praeorbulina-Orbulina*, *Globigerina-*  
516 *Globigerinella*, *Neogloquadrina*, *Pulleniatina*, *Sphaeroidinellopsis-Sphaeroidinella* (Fig. 6). We





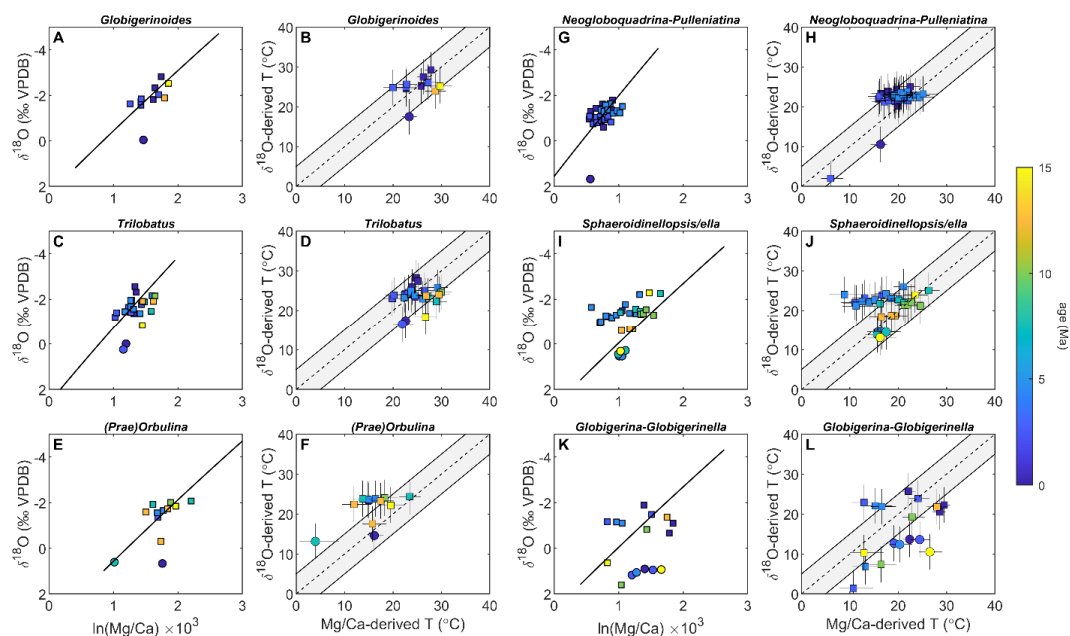
517 find that using a “nearest descendant” approach in the choice of temperature calibration improves  
 518 the agreement between  $\delta^{18}\text{O}$  and Mg/Ca temperatures for the neogloboquadrinids and  
 519 pulleniatinids (Fig. 7). At the same time, it enables us to identify “problematic” species and  
 520 lineages which require further investigations before being used for temperature reconstructions  
 521 (Fig. 7).



522

523 **Fig. 6**  $\delta^{18}\text{O}$  versus Mg/Ca and proxy-derived paleotemperature estimates for the ancestor-  
 524 descendent species *Globigerinoides subquadratus* – *G. ruber* (panels A and B), *Trilobatus trilobus*  
 525 – *T. sacculifer* (panels C and D), *Praeorbulina glomerosa* – *Orbulina suturalis* – *O. universalis*  
 526 (panels E and F), *Neogloboquadrina acostaensis* – *N. humerosa*, *N. pachyderma* – *N. incompta*,  
 527 *N. acostaensis* – *Pulleniatina primalis* – *P. praecursor* – *P. finalis* (panels G and H),  
 528 *Sphaeroidinellopsis seminulina* – *S. paenedehiscens* – *Sphaeroidinella dehiscens*, *S. seminulina* –  
 529 *S. kochi* (panels I and J), *Globigerinella praeshiphonifera* – *G. siphonifera* – *G. calida* and  
 530 *Globigerina bulloides* (panels K and L). Circle-symbols indicate data points from Site 516. Raw  
 531 proxy values are given with the long-term non-thermal controls on Mg/Ca subtracted out (as in  
 532 Fig. 2), as well as an estimate of paleotemperature (as in Fig. 3). The black lines depict one possible  
 533 estimate of the expected slope between  $\delta^{18}\text{O}$  and Mg/Ca (the blue line from Fig. 2), adjusted to  
 534 approximately match the location of the data by shifting them in the direction of  $\delta^{18}\text{O}$ . Datapoints  
 535 which are considered strongly affected by diagenesis are not included in this plot. Note that one  
 536 datapoint in panel G falls outside of the plot area.

537

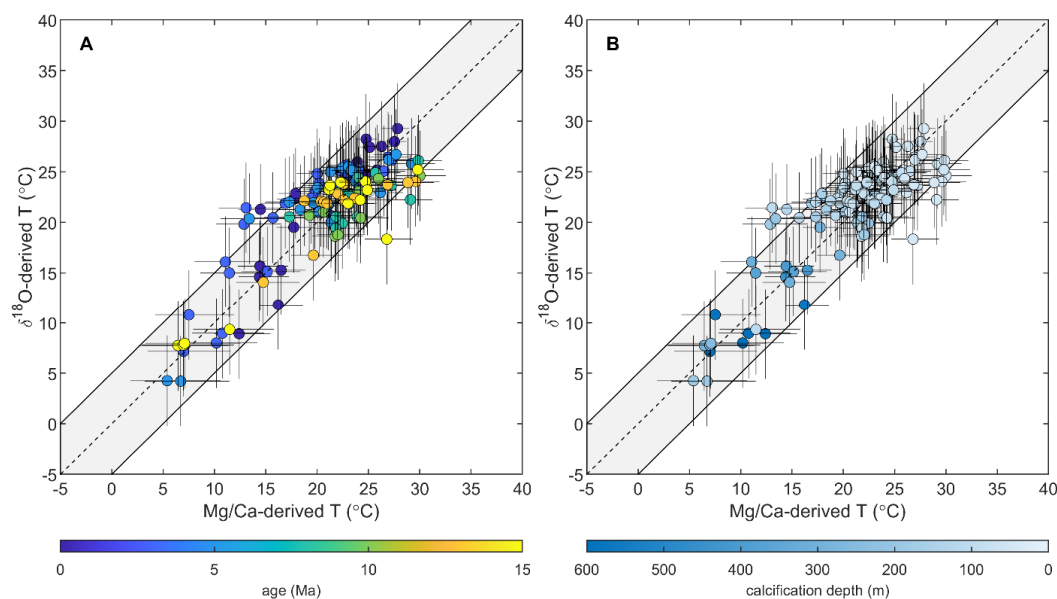


538

539 **Fig. 7.** As in Figure 4, except extending the use of species-specific calibrations to all species in a  
 540 lineage in the case of the *Trilobatus trilobus* – *T. sacculifer* (panels C and D), *Praeorbulina*  
 541 *glomerosa* – *Orbulina suturalis* – *O. universalis* (panels E and F), *Neogloboquadrina acostaensis* –  
 542 *N. humerosa*, *N. pachyderma* – *N. incompta*, *N. acostaensis* and between related lineages in the  
 543 case of *Neogloboquadrina* and the *Pulleniatina primalis* – *P. praecursor* – *P. finalis* lineage  
 544 (panels G and H).

545

546 Once all the potential sources of offset described above are taken into account, the species-specific  
 547 calibration for *Neogloboquadrina* is applied, and the data points which are still offset removed  
 548 from the dataset, the agreement between the two proxies increased from 62 to 91% of data points  
 549 falling within the combined uncertainties of the proxies (Fig. 8).



550

551 **Fig. 8.** As Fig. 3, with all offset lineages (§ 4.3; specifically, those that remain offset following the  
552 application of lineage-specific calibrations where possible) and diagenetically compromised (§  
553 3.1) samples removed. Removing these samples leaves 170 data points, of which 91% fall within  
554 the combined uncertainty of Mg/Ca- $\delta^{18}\text{O}$  agreement.

555

#### 556 **4.4. Planktonic foraminiferal Mg/Ca offsets as an expression of evolution**

557 The analysis of the Boscolo-Galazzo, Crichton et al. (2021) dataset performed here, allows offsets  
558 through ancestor-descendent species to be tracked for the first time, and the time of their  
559 appearance to be assessed. In this way, an attempt can be made to interpret offsets as the  
560 geochemical expression of evolutionary new biochemical pathways or ecological strategies in  
561 emerging species.

562 For spinose species, the observed high Mg/Ca offset is shared by ancestor-descendent species such  
563 as *Globigerinella praesiphonifera* - *G. siphonifera* and *Praeorbulina glomerosa* - *Orbulina*  
564 *suturalis* - *O. universa* (Fig. 4). *Globigerina bulloides* shares the same type of offset with



565 *Globigerinella* and a common ancestor (*Globigerina archaeobulloides*) in the earliest Oligocene  
566 (~33.5 Ma) (Spezzaferri et al., 2018) (Fig. 4), suggesting that for this group the offset may go back  
567 to at least the early globigerinids of the Paleogene. The genus *Praeorbulina* originated from the  
568 genus *Trilobatus* at about 16 Ma (Fig. 4) (Pearson et al., 1997; Aze et al., 2011). *Trilobatus trilobus*  
569 is the last common ancestor between the *Trilobatus* and *Praeorbulina-Orbulina* lineages (Fig. 4),  
570 and does not present offset Mg/Ca- $\delta^{18}\text{O}$  values, similar to its modern descendants (Figs. 4, 6). This  
571 suggests that the offset in *Praeorbulina-Orbulina* originated within the lineage and the  
572 morphological changes associated with it, and carried on to the modern representative *O. universa*.  
573 Spinose *Globigerinoides ruber* is also reported to be sensitive to pH changes (Kisakürek et al.,  
574 2008; Evans et al., 2016b), *G. ruber* is not offset in the analyzed dataset (both in the raw data and  
575 calculated temperatures), with ancestor-descendent *G. subquadratus-G. ruber* behaving similarly  
576 to the *Trilobatus trilobus* – *T. sacculifer* lineage through time (Figs 6-7), suggesting that this non-  
577 thermal effect is adequately accounted for in this case (Fig. 7) (i.e., the laboratory calibration are  
578 applicable downcore into deep-time in correcting for this). The on-average higher Mg/Ca  
579 displayed by offset spinose *Praeorbulina-Orbulina*, *Globigerinella* species and *G. bulloides* in the  
580 study dataset may suggest a lower pH environment which we cannot directly account for (Fig.  
581 2A). For *Globigerina* and *Globigerinella*, where a larger degree of scatter is observed (Fig. 6-7 K-  
582 L), the offset maybe linked to an opportunistic behavior and capability to adapt to a broad range  
583 of environmental conditions with variable pH (Weiner et al., 2015). This may in turn be related to  
584 the complexity of genotypes association in both *G. bulloides* and *Globigerinella* species, with  
585 different genotypes having different ecologies but almost identical morphologies (e.g., Weiner et  
586 al., 2015; Morard et al., 2024).



587 We find that the low Mg/Ca offset is shared between ancestor-descendent lineages  
588 *Neogloboquadrina-Pulleniatina* but possibly not between the lineages *Paragloborotalia-*  
589 *Neogloboquadrina* and is not shared between *Sphaeroidinellopsis-Sphaerodinella* (Fig. 5).  
590 *Neogloboquadrina* evolved from *Paragloborotalia continua*, in the late Miocene, at about 10  
591 Ma (Fig. 5). While paired Mg/Ca –  $\delta^{18}\text{O}$  measurements for *P. continua* are not available, paired  
592 Mg/Ca –  $\delta^{18}\text{O}$  measurements for *Paragloborotalia siakensis*, a species older than *P. continua*, do  
593 not show a low Mg/Ca offset (Supplementary Table 1). This may indicate either that the occurrence  
594 of low Mg/Ca crust/cortex started with *P. continua*, the youngest representative of the genus  
595 *Paragloborotalia* in our study, or with the neogloboquadrinids. The genus *Pulleniatina* evolved  
596 from *Neogloboquadrina acostaensis* at about 6.5 Ma (Pearson et al., 2023) (Fig. 5), by modifying  
597 the chambers arrangement and progressively developing a cortex. *Pulleniatina* may have inherited  
598 the capability to thicken its test from *Neogloboquadrina* and modified it into a cortex (Pearson et  
599 al., 2023). The occurrence of a low Mg/Ca cortex in *Pulleniatina* appears to start from the most  
600 ancient representative of this group, *P. primalis* (Figs. 5-6) and continues to the modern. Similar  
601 to *Paragloborotalia*, middle Miocene *Sphaeroidinellopsis kochi* and *S. seminulina* are not  
602 characterized by an offset to low Mg/Ca values. Nonetheless, an offset is observed in 5/10  
603 specimens for late Miocene – early Pliocene *S. paenedehiscens*, and always occurs for its  
604 descendent *Sphaerodinella dehiscens* (Fig. 7). Our analysis shows how the occurrence of a low  
605 Mg/Ca offset in planktonic foraminifera becomes progressively rarer going back in time, in  
606 parallel with the rarity of crust/cortex features. The occurrence of a crust/cortex is commonly  
607 observed in non-spinose modern planktonic foraminifera, however, only two early to middle  
608 Miocene genera are known to produce crusts (*Globoconella* and *Paragloborotalia*) and only one  
609 is known to produce cortex (*Sphaeroidinellopsis*).



610 It is tempting to put the pattern of emergence of Mg/Ca offsets in relationship with changes in  
611 ocean chemistry and global climate over the last 15 Myr. In particular, the offset spinose species  
612 are mostly tropical and evolved during a time when mean ocean pH was more than 0.1 pH unit  
613 lower than preindustrial (Rae et al., 2021). Further, the *Preorbulina* - *Orbulina* plexus evolved at  
614 about 16 Ma, in coincidence with a drop in ocean pH likely linked to the global warmth of the  
615 Miocene Climatic Optimum (Rae et al., 2021). The particularly high Mg/Ca signature of this group  
616 of species, along with their evolutionary timing, may testify their ability to withstand tropical  
617 surface waters more undersaturated than today thanks to changes in the biomineralisation pathway  
618 as a consequence of their evolution during the Miocene Climatic Optimum.

619 The evolution of the offset non-spinose species happened several millions of years later during the  
620 long-term cooling trend of the last 10 Myr. The offset species occur across tropical to high latitude  
621 areas and mixed-layer (*Sphaeroidinellopsis*, *Sphaeroidinella*) to intermediate (*Neogloboquadrina*,  
622 *Pulleniatina*) depth habitats. The ability to develop crust/cortex in species evolving over the last  
623 10 Myr might have been of advantage as the global ocean was becoming progressively colder and  
624 denser, in a similar way to the observed increases in shell-mass across Pleistocene glacial cycles  
625 (e.g., Zarcogiannis et al., 2019).

626 The last 10 Myr were also characterized by decreasing concentration in  $Ca_{sw}$  ( $[Ca^{2+}]$ ) in step with  
627 global cooling, reaching concentrations half those of the middle Miocene in the modern (Zhou et  
628 al., 2021). As a consequence,  $Mg/Ca_{sw}$  doubled over the past 5 Ma (Evans et al., 2016b). With  
629 decreasing  $[Ca^{2+}]$  and increasing  $[Mg^{2+}]$  in seawater over the Neogene (Brennan et al., 2013; Evans  
630 et al., 2016b; Zhou et al., 2021), some species may have started to more actively control the Mg/Ca  
631 ratio at their biomineralisation site, e.g., by proportionally decreasing the active transport of  $Mg^{2+}$ ,  
632 in order to buffer against the effects of the higher seawater Mg/Ca, and to keep the outer parts of



633 their shell with low Mg/Ca and thus more resistant to dissolution. Hence, the low Mg/Ca offset  
634 observed in the modern and fossils non-spinose species above might be linked to their evolutionary  
635 emergence during a time of changing ocean physical-chemical properties, which may have  
636 promoted the evolution of thicker tests with a different elemental chemistry making them less  
637 buoyant and resistant to dissolution.

## 638 **5. Conclusions**

639 We analyzed a multispecies planktonic foraminiferal  $\delta^{18}\text{O}$  and Mg/Ca dataset spanning the last 15  
640 million years at multiple locations to test whether temperature is the main controller of both proxies  
641 and assess the major overprinting factors through time, space and for species with very distinct  
642 ecologies. Once diagenesis and possible regional hydrographic factors are taken into account, we  
643 find that species-specific offsets not accounted for in our calibration strategy remain a source of  
644 mismatch between the two proxies. Specifically, *Globigerina*, *Globigerinella*, *Praeorbulina* and  
645 *Orbulina* species are consistently offset, with Mg/Ca values on average higher than expected.  
646 Conversely, non-spinose *Neogloboquadrina*, *Pulleniatina* and *Sphaeroidinellpsis-Sphaeroidinella*  
647 appear consistently offset with low Mg/Ca. The appearance of these geochemical offsets is linked  
648 to the origination of new clades, and is then shared between ancestor-descendent species, such that  
649 we were able to track their evolutionary history. The variable offset in *Globigerinella* may go back  
650 to the early globigerinids of the Paleogene and is probably related to the opportunistic behavior of  
651 this group leading to a wider-range of habitat conditions. The high Mg/Ca offset in *Orbulina* starts  
652 with *Praeorbulina* in the middle Miocene, while a low Mg/Ca offset is typical of groups evolving  
653 in the late Neogene characterized by a crust or cortex. This pattern suggests that the offsets  
654 observed in modern species may be a legacy of their parent groups originating millions of years  
655 ago, when ocean properties were different from today.



656 Overall, our study highlights the power of the multispecies and multi-time slice dataset presented  
657 here, enabling us to identify the evolutionary origin and timing of deviations in Mg/Ca-  
658 temperature/pH relationships. Furthermore, our study demonstrates the robustness of Mg/Ca and  
659  $\delta^{18}\text{O}$  proxies through geologic time when nonthermal factors (especially Mg/Ca<sub>sw</sub> and pH) are  
660 accounted for. For example, virtually all *Globigerinoides* and *Trilobatus* Mg/Ca and  $\delta^{18}\text{O}$ -derived  
661 temperature are within uncertainty of each other, highlighting the utility of these species for  
662 paleoceanographic reconstruction. In addition, our analysis enables us to identify species/lineages  
663 that should be treated with caution when interpreting Mg/Ca data, at the very least demonstrating  
664 that care should be taken in selecting the calibration approach and highlighting the need for further  
665 work in understanding the nonthermal controls on Mg incorporation into the shells of these  
666 foraminifera.

#### 667 **Code and Data availability**

668 All data are available as supplementary material of this paper. R and Matlab code to perform the  
669 ‘MgCaRB’ protocols are available on Github: <https://github.com/willyrgray/> MgCaRB for R,  
670 <https://github.com/dbjevans/MgCaRB> for Matlab.

#### 671 **Author contributions**

672 E.M.M. performed trace element analysis; F.B.G conceptualized the paper; D.E. performed data  
673 analysis; F.B.G and D.E. produced the figures; F.B.G and D.E. wrote the paper with contributions  
674 from all authors.

#### 675 **Competing interests**

676 The authors declare no competing interests.





677 **Acknowledgments**

678 This study was funded by Natural Environment Research Council (NERC) grant NE/N001621/1  
679 to P.N.P. (F.B.G.); NERC grant NE/P016375/1 to participate in IODP Expedition 363 (P.N.P.);  
680 and NERC grant NE/N002598/1 to B.S.W. (E.M.M.). Marcin Latas assisted with sample  
681 preparation funded by an EU Marie Curie Career Integration Grant 293741 to B.S.W; F.B.G  
682 acknowledges support from Horizon 2020 Framework Programme (H2020-MSCA-IF-2020  
683 101019438).

684 **References**

- 685 1. Anand, P., Elderfield, H., and Conte, M.H.: Calibration of Mg/Ca thermometry in  
686 planktonic foraminifera from a sediment trap time series, *Paleoceanography* 18, 1050,  
687 10.1029/2002PA000846, 2003.
- 688 2. Aze, T., Ezard, T.H.G., Purvis, A., Coxall, H.K., Stewart, D.R.M., Wade, B.S., and  
689 Pearson, P.N.: A phylogeny of Cenozoic macroperforate planktonic foraminifera from  
690 fossil data, *Biological Reviews* 86, 900–927, 10.1111/j.1469-185X.2011.00178, 2011.
- 691 3. Barker, S., Greaves, M., and Elderfield, H.: A study of cleaning procedures used for  
692 foraminiferal Mg/Ca paleothermometry, *Geochemistry, Geophysics, Geosystems* 4,  
693 10.1029/2003GC000559, 2003.
- 694 4. Birch, H., Coxall, H.K., Pearson, P.N., Kroon, D., and O'Regan, M.: Planktonic  
695 foraminifera stable isotopes and water column structure: Disentangling ecological signals,  
696 *Marine Micropaleontology* 10, 127–145, 10.1016/j.marmicro.2013.02.002, 2013.
- 697 5. Boscolo-Galazzo, F., Crichton, K.A., Ridgwell, A., Mawbey, E.M., Wade, B.S., and  
698 Pearson P.N.: Temperature controls carbon cycling and biological evolution in the ocean  
699 twilight zone, *Science*, 371, 1148–1152, 10.1126/science.abb6643, 2021.



- 700 6. Boscolo-Galazzo, F., Jones, A., Dunkley Jones, T., Crichton, K.A., Wade, B.S., and  
701 Pearson, P.N.: Late Neogene evolution of modern deep-dwelling plankton,  
702 Biogeosciences, 19, 743-762, doi.org/10.5194/bg-19-743-2022, 2022.
- 703 7. Branson, O., Read, E., Redfern, S. A. T., Rau, C., and Elderfield, H.: Revisiting diagenesis  
704 on the Ontong Java Plateau: Evidence for authigenic crust precipitation in *Globorotalia*  
705 *tumida*, Paleocyanography 30, 1490–1502, 10.1002/2014PA002759, 2015.
- 706 8. Brennan, S.T., Lowenstein, T.K., and Cendon, D.I.: The major-ion composition of  
707 Cenozoic seawater: the past 36 million years from fluid inclusions in marine halite,  
708 American Journal of Science 313, 713–775, doi.org/10.2475/08.2013.01, 2013.
- 709 9. Burke, K.D., Williams, J.W., Chandler, M.A., Haywood, A.M., Lunt, D.J., and Otto-  
710 Bliesner, B.L.: Pliocene and Eocene provide best analogs for near-future climates,  
711 Proceedings of the National Academy of Sciences 115, 13288-13293,  
712 doi.org/10.1073/pnas.1809600115, 2018.
- 713 10. Chave, K. E.: Aspects of the biogeochemistry of magnesium 1. Calcareous marine  
714 organisms, The Journal of Geology, 62, 266-283, 10.1086/626162, 1954.
- 715 11. Davis, C.V., Fehrenbacher, J.S., Hill, T.M., Russell, A.D., and Spero, H.J.: Relationships  
716 between temperature, pH, and crusting on Mg/Ca ratios in laboratory-grown  
717 Neogloboquadrina foraminifera, Paleocyanography 32, 2017PA003111,  
718 10.1002/2017PA003111, 2017.
- 719 12. Dekens, P.S., Lea, D.W., Pak, D.K., and Spero, H.J.: Core top calibration of Mg/Ca in  
720 tropical foraminifera: Refining paleotemperature estimation, Geochemistry, Geophysics,  
721 Geosystems 3, 1-29, 10.1029/2001GC000200 2002.



- 722 13. Edgar, K.M., Anagnostou, E., Pearson, P.N., and Foster, G.L.: Assessing the impact of  
723 diagenesis on  $\delta^{11}\text{B}$ ,  $\delta^{13}\text{C}$ ,  $\delta^{18}\text{O}$ , Sr/Ca and B/Ca values in fossil planktic foraminiferal  
724 calcite, *Geochimica et Cosmochimica Acta* 166, 189–209, 10.1016/j.gca.2015.06.018,  
725 2015.
- 726 14. Eggins S. M., Sadekov A. and De Deckker P.: Modulation and daily banding of Mg/Ca in  
727 *Orbulina universa* tests by symbiont photosynthesis and respiration: a complication for  
728 seawater thermometry? *Earth Planetary Science Letters* 225, 411–419,  
729 10.1016/j.epsl.2004.06.019, 2004.
- 730 15. Elderfield, H., and Ganssen, G.: Past temperature and  $\delta^{18}\text{O}$  of surface ocean waters  
731 inferred from foraminiferal Mg/Ca ratios, *Nature* 405, 442, 10.1038/35013033, 2004.
- 732 16. Elderfield, H., Yu, J., Anand, P., Kiefer, T., and Nyland, B.: Calibrations for benthic  
733 foraminiferal Mg/Ca paleothermometry and the carbonate ion hypothesis, *Earth and*  
734 *Planetary Science Letters* 250, 633–649, 10.1016/j.epsl.2006.07.041, 2006.
- 735 17. Emiliani, C.: Depth habitats of some species of pelagic foraminifera as indicated by oxygen  
736 isotope ratios, *American Journal of Science* 252, 149–158, 1954.
- 737 18. Erez, J., and Luz, B.: Experimental paleotemperature equation for planktonic foraminifera,  
738 *Geochimica et Cosmochimica Acta* 47, 1025 – 1031, 10.1016/0016-7037(83)90232-6,  
739 1983.
- 740 19. Evans D., Erez J., Oron S. and Muller W.: Mg/Ca temperature and seawater-test chemistry  
741 relationships in the shallow-dwelling large benthic foraminifera *Operculina ammonoides*,  
742 *Geochimica and Cosmochimica Acta* 148, 325–342, 10.1016/j.gca.2014.09.039, 2015.
- 743 20. Evans, D., Wade, B.S., Henehan, M., Erez, J., and Müller, W.: Revisiting carbonate  
744 chemistry controls on planktic foraminifera Mg/Ca: Implications for sea surface



- 745 temperature and hydrology shifts over the Paleocene-Eocene Thermal Maximum and  
746 Eocene-Oligocene transition, *Climate of the Past* 12, 819–835, 10.5194/cp-12-819-2016,  
747 2016a.
- 748 21. Evans, D., Brierley, C., Raymo, M.E., Erez, J., and Müller, W.: Planktic foraminifera shell  
749 chemistry response to seawater chemistry: Pliocene–Pleistocene seawater Mg/Ca,  
750 temperature and sea level change, *Earth and Planetary Science Letters* 438, 139-148,  
751 2016b, 10.1016/j.epsl.2016.01.013.
- 752 22. Fabbrini, A., Zaminga, I., Ezard, T. and Wade, B.S.: Systematic taxonomy of middle  
753 Miocene *Sphaeroidinellopsis* (planktonic foraminifera), *Journal of Systematic*  
754 *Palaeontology*, 19, 953-968, 10.1080/14772019.2021.1991500, 2021.
- 755 23. Fayolle, F. and Wade, B.S.: Data report: Miocene planktonic foraminifers  
756 *Dentoglobigerina* and *Globoquadrina* from IODP Sites U1489 and U1490, Expedition  
757 363. In: Rosenthal, Y., Holbourn, A.E., Kulhanek, D.K., and the Expedition 363 Scientists,  
758 Western Pacific Warm Pool. Proceedings of the International Ocean Discovery Program,  
759 363: College Station, TX (International Ocean Discovery Program),  
760 10.14379/iodp.proc.363.203.2020, 2020.
- 761 24. Friedrich, O., Schiebel, R., Wilson, P.A., Weldeab, S., Beer, C.J., Cooper, M.J., and Fiebig,  
762 J.: Influence of test size, water depth, and ecology on Mg/Ca, Sr/Ca,  $\delta^{18}\text{O}$  and  $\delta^{13}\text{C}$  in  
763 nine modern species of planktic foraminifers, *Earth and Planetary Science Letters* 319,  
764 133-145, 10.1016/j.epsl.2011.12.002, 2012.
- 765 25. Fritz-Endres, T., and Fehrenbacher, J.: Preferential loss of high trace element bearing inner  
766 calcite in foraminifera during physical and chemical cleaning, *Geochemistry, Geophysics,*  
767 *Geosystems*, 22, e2020GC009419, 10.1029/2020GC009419, 2021.



- 768 26. Gaskell, D.E., and Hull, P.: Technical note: A new online tool for  $\delta^{18}\text{O}$ –temperature  
769 conversions, *Climate of the past* 19, 1265–1274, 10.5194/cp-19-1265-2023, 2023.
- 770 27. Gaskell, D.E., Huber, M., O’Brien, C.L., Inglis, G.N., Acosta, R.P., Poulsen, C.J., and Hull,  
771 P.M.: The latitudinal temperature gradient and its climate dependence as inferred from  
772 foraminiferal  $^{18}\text{O}$  over the past 95 million years, *Proceedings of the National Academy of*  
773 *Science USA* 119, e2111332119, 10.1073/pnas.2111332119, 2022.
- 774 28. Gray, W.R., and Evans, D.: Nonthermal influences on Mg/Ca in planktonic foraminifera:  
775 A review of culture studies and application to the last glacial maximum, *Paleoceanography*  
776 *and Paleoclimatology* 34, 306–315, 10.1029/2018PA003517, 2019.
- 777 29. Gray, W. R., Weldeab, S., Lea, D. W., Rosenthal, Y., Gruber, N., Donner, B., and Fischer,  
778 G.: The effects of temperature, salinity, and the carbonate system on Mg/Ca in  
779 *Globigerinoides ruber* (white): A global sediment trap calibration, *Earth and Planetary*  
780 *Science Letters* 482, 607–620, 10.1016/j.epsl.2017.11.026, 2018.
- 781 30. Holland, K., Branson, O., Haynes, L.L., Honisch, B., Allen, K.A., Russell, A.D.,  
782 Fehrenbacher, J.S., Spero, H.J., and Eggins S.M.: Constraining multiple controls on  
783 planktic foraminifera Mg/Ca, *Geochimica et Cosmochimica Acta* 273, 116–136,  
784 10.1016/j.gca.2020.01.015, 2020.
- 785 31. Hönisch, B., Allen, K.A., Lea, D.W., Spero, H.J., Eggins, S.M., Arbuszewski, J., deMenocal,  
786 P., Rosenthal, Y., Russell, A.D., and Elderfield, H.: The influence of salinity on Mg/Ca  
787 in planktic foraminifers – evidence from cultures, core-top sediments and complementary  
788  $\delta^{18}\text{O}$ , *Geochim. Cosmochim. Acta* 121, 196–213, 10.1016/j.gca.2013.07.028, 2013.



- 789 32. Huber, B.T., Petrizzo, M.R., Young, J., Falzoni, F., Gilardoni, S., Bown, P.R., and Wade,  
790 B.S.: Pforams@mikrotax: A new online taxonomic database for planktonic foraminifera,  
791 *Micropalaeontology*, 62: 429-438, 2016.
- 792 33. John, E.H., Staudigel, P.T., Buse, B., Lear, C.H., Pearson, P.N., and Slater, S.M.: Revealing  
793 their true stripes: Mg/Ca banding in the Paleogene planktonic foraminifera genus  
794 *Morozovella* and implications for paleothermometry, *Paleoceanography and*  
795 *Paleoclimatology*, 38, e2023PA004652, 10.1029/2023PA004652, 2023.
- 796 34. Jonkers, L., de Nooijer, L.J., Reichart, G.-J., Zahn, R., and Brummer, G.-J.A.: Encrustation  
797 and trace element composition of *Neogloboquadrina dutertrei* assessed from single  
798 chamber analyses – implications for paleotemperature estimates, *Biogeosciences*, 9, 4851–  
799 4860, 10.5194/bg-9-4851-2012, 2012.
- 800 35. Jonkers, L., Gopalakrishnan, A., Weßel, L., Chiessi, C. M., Groeneveld, J., Monien, P., et  
801 al.: Morphotype and crust effects on the geochemistry of *Globorotalia inflata*,  
802 *Paleoceanography and Paleoclimatology* 36, e2021PA004224, 10.1029/2021PA004224 ,  
803 2021.
- 804 36. Kısakürek, B., Eisenhauer, A., Böhm, F., Garbe-Schönberg, D., and Erez, J.: Controls on  
805 shell Mg/Ca and Sr/Ca in cultured planktonic foraminiferan, *Globigerinoides ruber*  
806 (white), *Earth and Planetary Science Letters* 273, 260-269, 10.1016/j.epsl.2008.06.026,  
807 2008.
- 808 37. LeGrande A.N., and Schmidt G.A.: Global gridded data set of the oxygen isotopic  
809 composition in seawater, *Geophys. Res. Lett.* 33, L12604, 10.1029/2006GL026011, 2006.



- 810 38. Lea, D.W., Mashiotta, T.A., and Spero, H.J.: Controls on magnesium and strontium uptake  
811 in planktonic foraminifera determined by live culturing, *Geochimica et Cosmochimica*  
812 *Acta* 63, 2369-2379, 10.1016/S0016-7037(99)00197-0, 1999.
- 813 39. Lear, C.H., Rosenthal, Y., and Slowey, N.: Benthic foraminiferal Mg/Ca-  
814 paleothermometry: A revised core-top calibration, *Geochimica et Cosmochimica Acta* 66,  
815 3375-3387, 10.1016/S0016-7037(02)00941-9, 2002.
- 816 40. Leckie, R.M., Wade, B.S., Pearson, P.N., Fraass, A.J., King, D.J., Olsson, R.K., Premoli  
817 Silva, I., Spezzaferri, S., and Berggren, W.A.: Taxonomy, biostratigraphy, and phylogeny  
818 of Oligocene and early Miocene *Paragloborotalia* and *Parasubbotina*, in Wade, B.S.,  
819 Olsson, R.K., Pearson, P.N., Huber, B.T. and Berggren, W.A., *Atlas of Oligocene*  
820 *Planktonic Foraminifera*, Cushman Foundation of Foraminiferal Research, Special  
821 Publication, No. 46, p. 125-178, 2018.
- 822 41. Locarnini, R. A., Mishonov, A.V., Antonov, J.I., Boyer, T.P., Garcia, H.E., Baranova,  
823 O.K., Zweng, M.M., Paver, C.R., Reagan, J.R., Johnson, D.R., Hamilton, M., and Seidov,  
824 D.: *World Ocean Atlas 2013, Volume 1: Temperature*. S. Levitus, Ed., A. Mishonov  
825 Technical Ed.; NOAA Atlas NESDIS 73, 40 pp.
- 826 42. Lourens, L.J., Hilgen, F.J., Shackleton, N.J., Laskar, J., and Wilson, D.: The Neogene  
827 Period. In: Gradstein, F.M., Ogg, J.G., Smith, A.G. (Eds.), *Geological Time Scale 2004*.  
828 Cambridge University Press, pp. 409–440, 2004.
- 829 43. Malevich, S. B., Vetter, L., and Tierney, J. E.: Global Core Top Calibration of 18O in  
830 Planktic Foraminifera to Sea Surface Temperature, *Paleoceanography and*  
831 *Paleoclimatology*, 34, 1292–1315, 10.1029/2019PA003576, 2019.



- 832 44. Mathien-Blard, E., and Bassinot, F.: Salinity bias on the foraminifera Mg/Ca thermometry:  
833 correction procedure and implications for past ocean hydrographic reconstructions,  
834 *Geochem. Geophys. Geosyst.* 10, Q12011, 10.1029/2008GC002353, 2009.
- 835 45. McConnell, M.C., and Thunell, R.C.: Calibration of the planktonic foraminiferal Mg/Ca  
836 paleothermometer: sediment trap results from the Guaymas Basin, Gulf of California.  
837 *Paleoceanography* 20, PA2016, 10.1029/2004PA001077, 2005.
- 838 46. Miller, K.G., Kominz, M.A., Browning, J.V., Wright, J.D., Mountain, G.S., Katz, M.E.,  
839 Sugarman, P.J., Cramer, B.S., Christie-Blick, N., and Pekar, S.F.: The Phanerozoic record  
840 of global sea-level change, *Science* 310, 1293–1298, 10.1126/science.1116412, 2005.
- 841 47. Morard, R., Darling, K.F., Weiner, A.K.M., Hassenrück, C., Vanni, C., Cordier, T., Henry,  
842 N., Greco, M., Vollma, N.M., Milivojevic, T., Rahman, S.N., Siccha, M., Meilland, J.,  
843 Jonkers, L., Quillévéré, F., Escarguel, G., Douady, C.J., de Garidel-Thoron, T., de Vargas,  
844 C., and Kucera, M.: The global genetic diversity of planktonic foraminifera reveals the  
845 structure of cryptic speciation in plankton, *Biological Reviews*, 10.1111/brv.13065, 2024.
- 846 48. Mucci, A.: Influence of temperature on the composition of magnesian calcite overgrowths  
847 precipitated from seawater, *Geochimica et Cosmochimica Acta* 51, 1977-1984,  
848 10.1016/0016-7037(87)90186-4, 1987.
- 849 49. Mucci, A., Morse, J.W.: The incorporation of Mg<sup>2+</sup> and Sr<sup>2+</sup> into calcite overgrowths:  
850 influences of growth rate and solution composition, *Geochimica et Cosmochimica Acta*  
851 47, 217-233, 10.1016/0016-7037(83)90135-7, 1983.
- 852 50. Nuernberg, D.: Magnesium in tests of *Neogloboquadrina pachyderma* sinistral from high  
853 northern and southern latitudes, *The Journal of Foraminiferal Research* 25, 350-368,  
854 10.2113/gsjfr.25.4.350, 1995.





- 855 51. Nürnberg, D., Bijma, J., and Hemleben, C.: Assessing the reliability of magnesium in  
856 foraminiferal calcite as a proxy for water mass temperatures, *Geochimica et Cosmochimica*  
857 *Acta* 60, 803-814, 10.1016/0016-7037(95)00446-7, 1996.
- 858 52. Opdyke, B.N., and Pearson, P.N.: Data report: geochemical analysis of multiple planktonic  
859 foraminifer species at discrete time intervals, In: Haggerty, J.A., Premoli Silva, I., Rack,  
860 F., and McNutt, M.K. (Eds.), *Proceedings of the Ocean Drilling Program, Scientific*  
861 *Results*, 144, 993-995, 10.2973/odp.proc.sr.144.052.1995, 1995.
- 862 53. Pälike, H., Norris, R.D., Herrle, J.O., Wilson, P.A., Coxall, H.K., and Lear, C.H.,  
863 Shackleton, N.J., Tripathi, A.K., Wade, B.S.: The heartbeat of the Oligocene climate system,  
864 *Science* 314, 1894–1898, 10.1126/science.1133822, 2006.
- 865 54. Pearson, P.N., Shackleton, N.J., and Hall, M.A.: Stable isotopic evidence for the sympatric  
866 divergence of *Globigerinoides trilobus* and *Orbulina universa*, *Journal of the Geological*  
867 *Society*, 154, 295–302, 10.1144/gsjgs.154.2.0295, 1997.
- 868 55. Pearson, P.N.: Oxygen isotopes in foraminifera: overview and historical review. In  
869 *Reconstructing Earth's Deep-Time Climate, Paleontological Society Papers Volume 18*, L.  
870 Ivany, B. Huber, Eds. (2012), pp. 1–38, 2012.
- 871 56. Pearson, P.N., Young, J., King, D.J., and Wade, B.S.: Biochronology and evolution of  
872 *Pulleniatina* (planktonic foraminifera), *Journal of Micropalaeontology*, 42, 211–255,  
873 10.5194/jm-42-211-2023, 2023.
- 874 57. Rae, J.W.B., Zhang, Y., Liu, X., Foster, G.L., Stoll, H.M., and Whiteford, D.M.:  
875 Atmospheric CO<sub>2</sub> over the past 66 million years from marine archives, *Annual Review of*  
876 *Earth and Planetary Sciences* 49, 609–641, 10.1146/annurev-earth-082420-063026, 2021.



- 877 58. Regenberg, M., Regenberg, A., Garbe-Schönberg, D., and Lea, D.W.: Global dissolution  
878 effects on planktonic foraminiferal Mg/Ca ratios controlled by the calcite-saturation state  
879 of bottom waters, *Paleoceanography*, 29, 127–142, 10.1002/2013PA002492, 2014.
- 880 59. Rohling, E. J., Yu, J., Heslop, D., Foster, G. L., Opdyke, B., and Roberts, A. P.: Sea level  
881 and deep-sea temperature reconstructions suggest quasi-stable states and critical transitions  
882 over the past 40 million years, *Sci. Adv.* 7, eabf5326, 10.1126/sciadv.abf5326, 2021.
- 883 60. Rongstad, B.L., Marchitto, T.M., and Herguera, J.C.: Understanding the effects of  
884 dissolution on the Mg/Ca paleothermometer in planktic foraminifera: Evidence from a  
885 novel individual foraminifera method, *Paleoceanography* 32, 1386–1402,  
886 10.1002/2017PA003179, 2017.
- 887 61. Russell, A.D., Honisch, B., Spero, H.J., Lea, D.W.: Effects of seawater carbonate ion  
888 concentration and temperature on shell U, Mg, and Sr in cultured planktonic foraminifera,  
889 *Geochimica and Cosmochimica Acta* 68, 4347–4361, 10.1016/j.gca.2004.03.013, 2004.
- 890 62. Sexton, P.E., Wilson, P.A., and Pearson, P.N.: Microstructural and geochemical  
891 perspectives on planktic foraminiferal preservation: “Glassy” versus “Frosty”, *Geochem.*  
892 *Geophys. Geosyst.* 7, 10.1029/2006GC001291, 2006.
- 893 63. Schiebel, R., and Hemleben, C.: *Planktic foraminifers in the modern ocean*. Springer, 2017.
- 894 64. Spero, H.J., Bijma, J., Lea, D.W., Bemis, B.E.: Effect of seawater carbonate concentration  
895 on foraminiferal carbon and oxygen isotopes, *Nature* 390, 497–500, 10.1038/37333, 1997.
- 896 65. Spezzaferri, S., Coxall, H.K., Olsson, R.K., and Hemleben, C.: Taxonomy, biostratigraphy  
897 and phylogeny of Oligocene *Globigerina*, *Globigerinella*, and *Quiltyella* n. gen., in Wade,  
898 B.S., Olsson, R.K., Pearson, P.N., Huber, B.T. and Berggren, W.A., *Atlas of Oligocene*



- 899 Planktonic Foraminifera, Cushman Foundation of Foraminiferal Research, Special  
900 Publication, No. 46, p. 125-178, 2018.
- 901 66. Spratt, R.M., and Lisiecki, L.: A Late Pleistocene sea-level stack, *Climate of the past* 12,  
902 1070-1092, 10.5194/cp-12-1079-2016, 2016.
- 903 67. Staudigel, P.T., John, E.H., Buse, B., Pearson, P.N., and Lear, C.H.: Apparent preservation  
904 of primary foraminiferal Mg/Ca ratios and Mg-banding in recrystallized foraminifera,  
905 *Geology* 50, 760–764, 10.1130/G49984.1, 2022.
- 906 68. Tierney, J.E., Malevich, S.B., Gray, W., Vetter, L., and Thirumalai, K.: Bayesian  
907 calibration of the Mg/Ca paleothermometer in planktic foraminifera, *Paleoceanography*  
908 and *Paleoclimatology* 34, 2005-2030, 10.1029/2019PA003744, 2019.
- 909 69. Urey, H.C.: The thermodynamic properties of isotopic substance, *Journal of the Chemical*  
910 *Society of London* 1947, 562–581, 1947.
- 911 70. Urey, H.C. Oxygen isotopes in nature and in the laboratory, *Science* 108, 489–496, 1948.
- 912 71. Von Langen, P.J., Pak, D.K., Spero, H.J., and Lea, D.W.: Effects of temperature on Mg/Ca  
913 in neogloboquadrinid shells determined by live culturing, *Geochemistry, Geophysics,*  
914 *Geosystems* 6, 10.1029/2005GC000989, 2005.
- 915 72. Wade, B.S., Pearson, P.N., Berggren, W.A., and Pälike, H.: Review and revision of  
916 Cenozoic tropical planktonic foraminiferal biostratigraphy and calibration to the  
917 geomagnetic polarity and astronomical time scale, *Earth-Science Reviews* 104, 111-142,  
918 10.1016/j.earscirev.2010.09.003, 2011.
- 919 73. Weiner, A.K.M., Weinkauf, M.F.G., Kurasawa, A., Darling, K.F., and Kucera, M.: Genetic  
920 and morphometric evidence for parallel evolution of the *Globigerinella calida*



- 921 morphotype, *Marine Micropaleontology* 114, 19–35, 10.1016/j.marmicro.2014.10.003,  
922 2015.
- 923 74. Westerhold, T., Marwan, N., Drury, A.J., Liebrand, D., Agnini, C., Anagnostou, E., Barnet,  
924 J.S.K., Bohaty, S.M., Vleeschouwer, D.D., Florindo, F., Frederichs, T., Hodell, D.A.,  
925 Holbourn, A. E., Kroon, D., Lauretano, V., Littler, K., Lourens, L.J., Lyle, M., Pälike, H.,  
926 Röhl, U., Tian, J., Wilkens, R.H., Wilson, P.A., and Zachos, J.C.: Anastronomically dated  
927 record of Earth’s climate and its predictability over the last 66 million years, *Science*, 369,  
928 1383–1387, 10.1126/science.aba6853, 2020.
- 929 75. Yu, J., Elderfield, H., Greaves, M., and Day, J.: Preferential dissolution of benthic  
930 foraminiferal calcite during laboratory reductive cleaning, *Geochemistry, Geophysics,*  
931 *Geosystems* 8, 10.1029/2006GC001571, 2007.
- 932 76. Zarkogiannis, S.D., Antonarakou, A., Tripathi, A., Kontakiotis, G., Mortyn, P.G., Drinia,  
933 H., and Greaves, M.: Influence of surface ocean density on planktonic foraminifera  
934 calcification, *Scientific Reports* 9, 10.1038/s41598-018-36935-7, 2019.
- 935 77. Zeebe, R. E.: An explanation of the effect of sea water carbonate concentration on  
936 foraminiferal oxygen isotopes, *Geochimica, Cosmochimica, Acta* 63, 2001–2007,  
937 10.1016/S0016-7037(99)00091-5, 1999.
- 938 78. Zeebe, R.E., and Tyrrell, T.: History of carbonate ion concentration over the last 100  
939 million years II: revised calculations and new data, *Geochimica and Cosmochima Acta*  
940 257, 373–392, 10.1016/j.gca.2019.02.041, 2019.
- 941 79. Zhou, X., Rosenthal, Y., Haynes, L., Si W., Evans, D., Huang, K.-F., Honisch, B., and  
942 Erez, J.: Planktic foraminiferal Na/Ca: A potential proxy for seawater calcium

<https://doi.org/10.5194/egusphere-2024-1608>

Preprint. Discussion started: 27 June 2024

© Author(s) 2024. CC BY 4.0 License.



943 concentration, *Geochimica et Cosmochimica Acta* 305, 306–322,

944 10.1016/j.gca.2021.04.012, 2021.